Hindawi
Geofluids
Volume 2022, Article ID 9410245, 24 pages
https://doi.org/10.1155/2022/9410245

Research Article

Thermo-Hydro-Mechanical Coupling Numerical Simulation on Mechanical Heterogeneity of Coal Rock

Shuiqing Hu,[1] Daobing Wang,[2] Yipeng Li,[3] Xiongfei Liu,[4] Fujian Zhou,[4] Meng Wang,[5] Chunming He,[5] and Bo Yu[2]

[1]*Tight Oil Research Institute, CNPC Research Institute of Petroleum Exploration & Development, Beijing 100083, China*
[2]*School of Mechanical Engineering, Beijing Institute of Petrochemical Technology, Beijing 102617, China*
[3]*Tuha Downhole Service Company, CNPC Western Drilling Engineering Company Limited, Hami 839009, China*
[4]*Unconventional Oil and Gas Science Technology Institute, China University of Petroleum-Beijing, Beijing 102249, China*
[5]*Fracturing and Acidizing Technical Center, CNPC Research Institute of Petroleum Exploration & Development, Beijing 100083, China*

Correspondence should be addressed to Daobing Wang; 0546wdb@163.com and Xiongfei Liu; lxfei@cup.edu.cn

Received 12 May 2022; Accepted 11 July 2022; Published 8 August 2022

Academic Editor: Wenming Ji

Coal rock is a porous medium composed of organic matter and inorganic minerals, and it is very complex and highly heterogeneous. Coal bed methane (CBM) production is a thermo-hydro-mechanical (THM) coupling process in heterogeneous coal rock. THM coupling numerical simulation on the coal rock by considering the effect of mechanical heterogeneity is rarely reported. We use Weibull's probability density distribution function to characterize the heterogeneity in elastic modulus of the coal rock, establish a THM coupling 3D finite element model of the coal rock by considering the variation in pore pressure caused by methane desorption, the linear thermal expansion effect, and coal rock skeleton shrinkage and deformation, and analyze variation in permeability, porosity, stress, temperature, and pore pressure within the coal rock representative elementary volume (REV) of variable mechanical heterogeneity with the cross-coupling correlation between permeability and porosity, and thermal field, stress field, and pressure field. The results show that the evolution of porosity and permeability in the coal rock is a THM coupling process related to mechanical heterogeneity, thermal expansion effect, pore pressure change caused by CBM desorption, and stressed deformation in the coal rock skeleton. The permeability and porosity fluctuate within the heterogeneous coal rock. The permeability and porosity fluctuate more frequently in the coal rock with stronger mechanical heterogeneity. The mechanical heterogeneity promotes local stress concentration. The time for variation in the stress through the whole the coal rock REV and the value of the first principal stress increase when the coal rock heterogeneity is enhanced. Under the THM coupling effect, the strong heterogeneity of the coal rock causes fluctuation in the thermal field. The evolution of coal porosity and permeability is a THM coupling process. This study provides theoretical guidance for CBM exploitation.

1. Introduction

China has an abundant CBM reserve, which is 30.05×10^{12} m^3, and is mainly hosted in Qinshui Basin and Ordos Basin [1, 2]. CBM is highly efficient and clean energy. CBM, shale gas, and tight sandstone gas are all unconventional gas [3]. CBM is stored as an adsorbed state in the coal bed. CBM exploitation is completed through desorption, diffusion, and seepage and is controlled by temperature, pore pressure, and in situ stress. Thus, CBM exploitation is essentially a THM coupling process. The THM multifield coupling process in the coal rock is a hot topic in CBM exploitation.

The THM coupling study is of great significance for accelerating gas desorption, improving coal rock permeability, and enhancing CBM recovery.

Previous experiments show that the coal rock permeability is closely related to confined pressure, temperature, and pore pressure. When the coal rock is heating up, the permeability generally shows a downward trend and is also possibly recovered. The variation in the coal rock permeability is the result of the coupling of matrix thermal expansion, gas desorption, and evaporation of residual water within cracks. Feng et al. [4] carried out experiments on mechanical deformation of anthracite in the process of heating from room temperature (i.e., 25°C) to 600°C and found the thermal effect on coal rock deformation in the thermal expansion stage from room temperature to 200°C, in the slow compression and deformation stage at 200-400°C, and in the strengthening compression stage at 400-600°C. The transition from brittle deformation to ductile deformation in anthracite occurs at 400-450°C. The thermal effect on the coal rock mechanical properties was tested under gas-free conditions, which is different from the underground gas-bearing conditions. In fact, the gas always exists dynamically within the coal rock. Due to gas desorption and adsorption in the coal rock, the effect of gas content on coal rock deformation is significant. The study shows that the adsorption capacity of CBM decays when the coal rock temperature rises. The temperature has a significant effect on coal rock's mechanical properties which are closely related to coal rank, deformation stage, and pore pressure.

Yin et al. [5] developed the true triaxial servo-controlled THM coupling seepage device for experiments on gas-bearing coal rock and carried out a study on the gas permeability in the gas-bearing coal rock during full stress-strain. The results show that the coal rock at a higher temperature has a lower compressive strength and experiences smaller failure strain and is more prone to failure. The gas permeability in the coal rock mainly depends on the stress-strain stage. In the stages of initial compression and linear elastic deformation in the coal rock, the gas permeability drops with increase of the deviatoric stress. In the stages of yield, failure, and residual deformation in the coal rock, the gas permeability increases with increase of the deviatoric stress. The thermal effect on the gas permeability varies during coal rock deformation, and it is more obvious before yield deformation, where the high temperature causes deterioration of permeability. After yield deformation of coal rock, a large number of microcracks are generated in the coal rock and have a great impact on the gas permeability, and the thermal effect on the gas permeability is weakened. Liu et al. [6] carried out a study on the effect of initial adsorption equilibrium pressure and temperature on gas migration in the coal rock in experiments on CBM desorption and diffusion. The results show that the higher temperature is favorable for gas desorption and diffusion, and the gas desorption consumes the heat in the coal rock and causes a temperature drop in the coal rock, which is adverse to gas desorption and diffusion. Cyclic loading affects coal rock permeability due to reversible deformation and damage and crack propagation. Cai et al. [7] monitored the evolution of the gas permeability in semianthracite and anthracite under triaxial cyclic loading through CT scanning, acoustic emission, and P-wave velocity methods. The memory of cracks occurs when the axial stress is unloaded, which is similar to the acoustic emission Kaiser effect. The gas permeability in the coal rock is related to fracture connectivity, geometry, and stress. During loading of stress in the coal rock, the permeability decreases, and the P-wave velocity increases. Huang et al. [8] developed a THM coupling triaxial device with the function of X-ray scanning, and the confining pressure, axial force, injected fluid pressure, and temperature are up to 20 MPa, 400 kN, 10 MPa, and 100°C, respectively. They carried out the experiment on the gas permeability during triaxial stress loading and unloading of coal rock. The results show that the fractures are mainly caused by expansion of initial fractures during cyclic loading of triaxial stress. The fracture area ratio in the coal rock increases linearly with the stress cycle. As the fracture area ratio increases, the gas permeability in the coal rock increases. The experimental results are affected by the size of the coal rock samples. In fact, the small size of rock samples in the laboratory cannot be exactly equivalent to the real situation in the field application, even though some similarity criterion is usually used in the experiment to reduce the errors. Some importance characteristics such as formation heterogeneity and anisotropy cannot be completely included in rock samples with small size.

A lot of efforts have been put into numerical simulation of gas flow in the coal rock. Yang et al. [9] established a gas seepage-stress coupling model by considering gas desorption and adsorption and carried out a simulation. The results show that the confining pressure has a great effect on gas drainage, and the high confining pressure causes strong resistance in the gas flow, which leads to low gas production. Nevertheless, the thermal effect on the gas permeability was ignored. Ma [10] established a THM coupling model of the coal rock by considering the thermal effect during gas extraction. The simulation results show that rising temperature significantly enhances gas desorption which in turn causes deformation of the coal rock, and this is beneficial to improve the gas permeability. Howerver, this model does not consider the effect of mechanical heterogeneity on the porosity and permeability of coal rock. Based on this THM model, Wei [11] established a 2D THM damage coupling model and studied the variation in in situ stress and evolution of coal damage under different lateral pressure coefficients and hole wall warming conditions. Tao et al. [12] established a real three-field and two-way THM coupling mathematical model by applying theories of elasticity, seepage mechanics, and heat transfer. This model reveals the internal relationship between the gas flow field, deformation field, and thermal field in the gas-bearing coal rock. They verified the model by comparing the experimental results to analytical solutions. Hosking et al. [13] proposed a dual pore THM coupling model of nonisothermal gas flow during CO_2 sequestration in the coal rock. The analytical solution and experimental results are compared to verify the reliability of the model. Xue et al. [14] developed a full THM coupling model which considers the nonlinear response of

CBM production and verified the reliability of the model by matching it with the historic data. Zhao et al. [15] modified the THM coupling model by considering internal expansion and deformation, corrected the equations describing coal rock deformation and permeability, and used the dynamic diffusion model to describe the evolution of gas diffusion in the coal rock matrix. Moreover, a new model of matrix porosity was introduced based on the assumption that the change in the pore volume equals that in the matrix volume. Zhu et al. [16] extended the dual permeability model to the damage mechanics of coal rock caused by gas adsorption and dissolution and obtain the change in permeability when CO_2, CH_4, and N_2 are injected into coal rock.

The heterogeneity of coal rock affects its mechanical properties. Wang et al. [17] carried out the uniaxial acoustic emission test on the black shale sampled at the depth of 1145 m from Well Youqian 1 in Chongqing and compared the results to those from coarse-grained granite samples. The shale samples show a significant difference in the wave velocity, strength, and brittleness, indicating strong microscopic heterogeneity. The total organic carbon content (TOC), mineral composition, and natural fractures are the main factors affecting the mechanical heterogeneity of shale. Wang et al. [18] applied Weibull's probability density function to describe the mechanical heterogeneity of shale and carried out a numerical simulation on the effects of the in situ stress distribution, strain energy density, fluid pressure, and damage of shale under hydro-mechanical coupling during hydraulic fracturing. Nevertheless, the thermal effect on shale damage was not considered. Zhu et al. [19] proposed a finite element method based on digital images for the study of the rock microscopic heterogeneity, obtained the effect of microscopic heterogeneity on the macroscale mechanical properties, defined the attribute graph according to the pixel ratio of digital imaging, and used the variable elastic modulus and permeability to describe rock heterogeneity. Nevertheless, the model is two-dimensional and cannot reflect the real spatial process.

Coal rock is highly heterogeneous. The effects of mechanical heterogeneity on the temporal and spatial evolution of gas permeability and porosity have been rarely reported. We use Weibull's probability density distribution function to characterize the elastic modulus heterogeneity of the coal rock, establish a 3D THM coupling finite element model by considering the pressure change caused by methane desorption, the linear thermal expansion effect, and the shrinkage and deformation of the coal rock skeleton, and analyze the variation in permeability and porosity in the coal rock REV with the cross-coupling correlation between the permeability and porosity and the thermal field, stress field, and pore pressure field.

The paper is organized as follows. Firstly, it provides the coal rock THM coupling physical model and assumptions. Secondly, it develops the governing equation, boundary conditions, finite element coupling algorithm of the THM coupling model, and random characterization methods of coal rock mechanical heterogeneity. Thirdly, it illustrates numerical simulation results, including case verification and sensitivity analysis. Finally, it describes the conclusions.

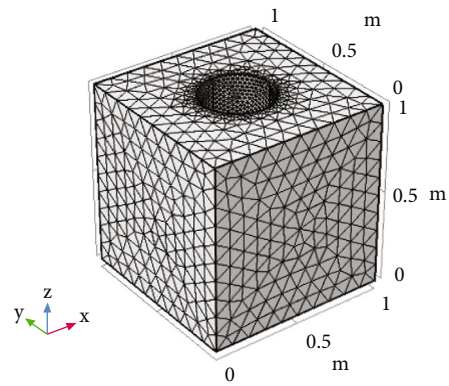

Figure 1: THM coupling finite element model of the coal rock during gas extraction.

2. Finite Element Model

The solution to the 3D THM coupling problem needs a huge computational cost. To save the computation cost, we establish a physical model in a $1\,\text{m} \times 1\,\text{m} \times 1\,\text{m}$ REV where a borehole with a radius of 0.2 m is set in the center. Here, the tetrahedral elements are used to mesh the RVE in the 3D space, and a total of 34,878 elements are generated. To simulate stress concentration around the borehole, local meshes are refined around the borehole (Figure 1). The discrete term of time derivative is expressed with an implicit format and an adaptive time step, and the Petrov-Galerkin finite element method ensures computational stability of the THM interaction model [20, 21]. The coal rock THM coupling finite element model is meshed (Figure 1). It is assumed that (1) the gas permeability is isotropic; (2) the fluid is slightly compressible, and the THM coupling effect on in situ stress, pore pressure, and temperature are considered; (3) the coal rock damage caused by variation in fluid pressure, rock deformation, and temperature is negligible; (4) the heterogeneity of thermal property is not considered in our simulation, and we only consider the mechanical heterogeneity of elastic modulus of coal rocks in this paper.

3. Mathematical Model

3.1. Mechanic Equation of Coal Rock Deformation. According to the theory of elastic mechanics, the mechanical equilibrium equation for coal rock deformation is expressed as follows:

$$\sigma_{ij,j} + f_i = 0. \tag{1}$$

Assuming that the coal rock is an isotropic medium and the coal rock is under linear elastic deformation, the stress-strain relation for coal rock deformation described by the Biot constitutive theory is expressed as follows:

$$\sigma_{ij} = 2G\varepsilon_{ij} + \frac{2G\mu}{1-2\mu}\varepsilon_{kk}\delta_{ij} - \alpha p\delta_{ij} - K\alpha_T T\delta_{ij} - K\varepsilon_s\delta_{ij}. \tag{2}$$

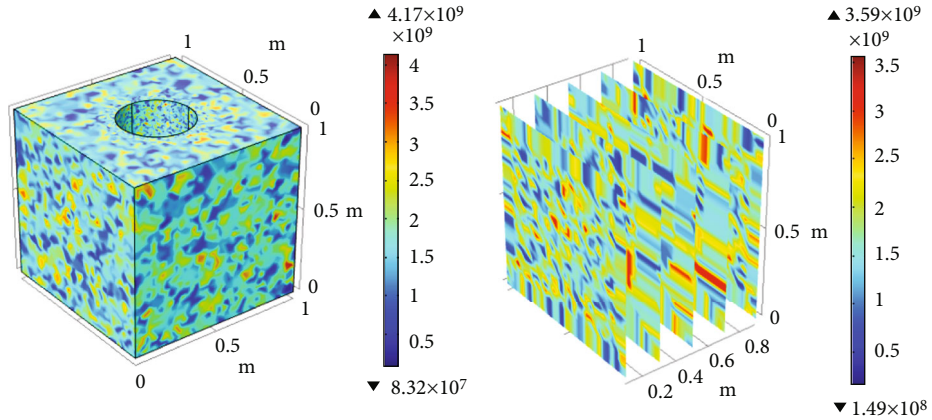

Figure 2: Three-dimensional (3D) mechanical heterogeneity characterization of coal rock: (a) 3D distribution of elastic modulus of coal rock (a) and (b) section of elastic modulus.

Table 1: Model parameters.

Parameters	Value
Initial porosity (decimal)	0.15
Initial pore pressure (MPa)	5
Poisson's ratio (decimal)	0.31
Skeleton bulk modulus (MPa)	166
Elastic modulus (GPa)	1.85
Coal rock density (kg/m^3)	1320
Thermal expansion coefficient (1/K)	1.16×10^{-4}
Initial permeability (m^2)	3.82×10^{-17}
Methane adsorption constant (a/m^3/kg)	14.5
Methane adsorption constant (b/1/MPa)	0.72
Methane adsorption constant (c/kg/m^3)	13.66
Molar gas constant (J/(mol·K))	8.341
Klingberg coefficient (Pa)	7.6×10^5
Gas molar volume (m^3/mol)	0.0224
Lamé's constant (λ/GPa)	1.1521
Lamé's constant (G/GPa)	0.70611
Methane density (kg/m^3)	0.714
Gas viscosity (Pa·s)	1.34×10^{-5}
Initial temperature (K)	273.15
Coal rock temperature (K)	293.15
Heat capacity ratio at constant pressure (J/(kg·K))	200

The relationship between strain and displacement in the deformed coal rock is expressed as follows:

$$\varepsilon_{ij} = \frac{1}{2}\left(u_{i,j} + u_{j,i}\right). \tag{3}$$

According to Equation (1), the volumetric strain is expressed as follows:

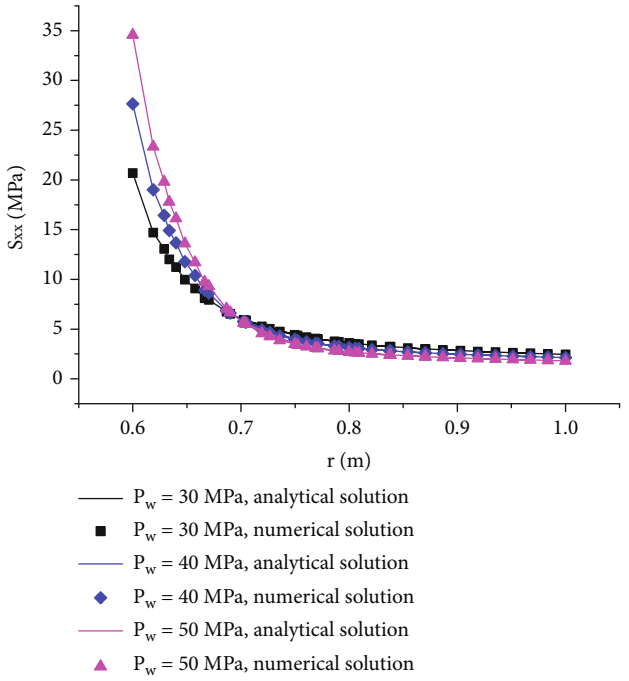

Figure 3: Numerical and analytical solutions to S_{xx} stress component.

$$\varepsilon_V = \frac{1}{K}(\bar{\sigma} + \alpha p) + \alpha_T T + \varepsilon_s, \tag{4}$$

where $\sigma_{eij} = \sigma_{ij} + \alpha p \delta_{ij}$.

The volumetric contraction strain of coal rock caused by gas desorption is defined as

$$\varepsilon_s = \alpha_{sg} V_{sg}. \tag{5}$$

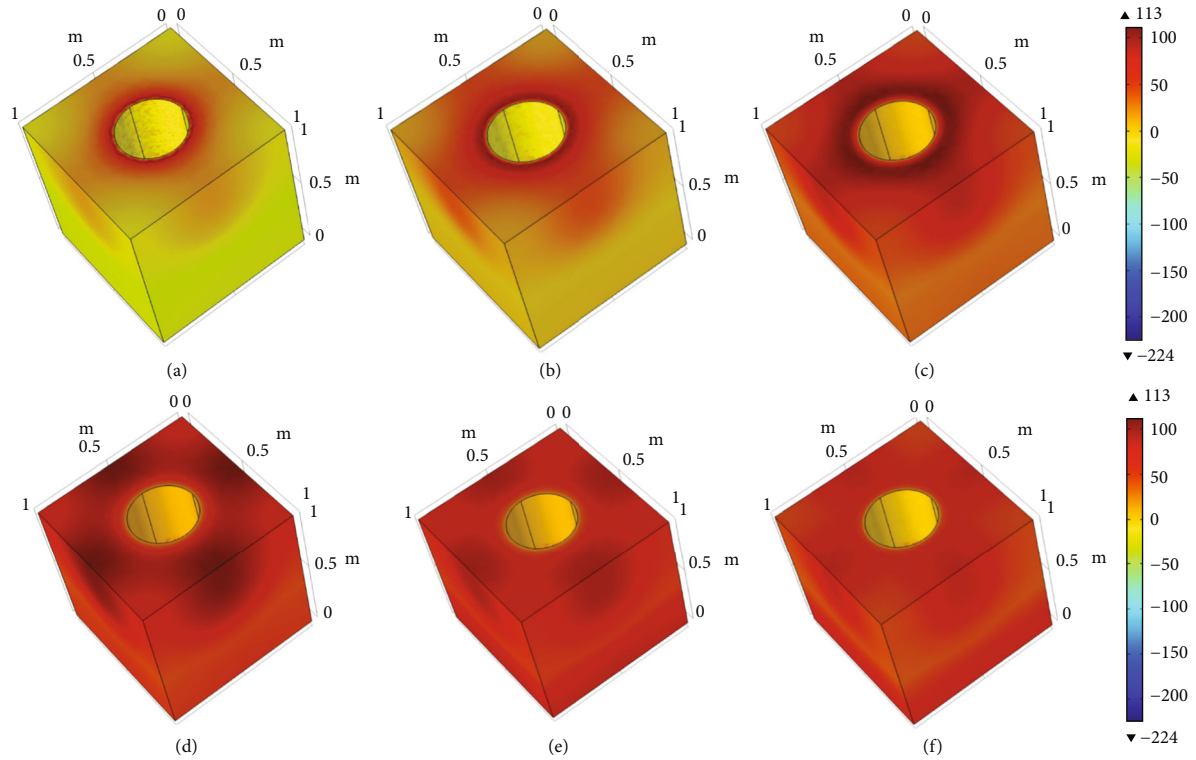

FIGURE 4: First principal stress field in the homogeneous coal rock: (a) $t = 0.1$ s, (b) $t = 1 \times 10^3$ s, (c) $t = 1 \times 10^4$ s, (d) $t = 1 \times 10^5$ s, (e) $t = 1 \times 10^6$ s, and (f) $t = 1 \times 10^7$ s.

By substituting Equations (2)–(5) into Equation (1), we obtain the differential equation of coal rock deformation as follows:

$$Gu_{i,jj} + \frac{G}{1-2\mu} u_{j,ji} - \alpha p_{,i} - K\alpha_T T_{,i} + f_i = 0. \tag{6}$$

The body force in Equation (6) is not considered in the next simulation because the THM coupling model is 2D, and thus, the value of the body force vector f_i is equal to zero in the numerical simulation.

3.2. Equation of Gas Seepage in the Coal Rock. According to the law of conservation of mass, the differential equation of gas seepage in the coal rock is expressed as follows:

$$\frac{\partial m}{\partial t} + \nabla\left(\rho_g \mathbf{v}_g\right) = Q_s. \tag{7}$$

According to the Langmuir equation, the content of methane gas adsorbed in the coal matrix is expressed as follows:

$$m = \rho_g \phi + \rho_{ga} \rho_c V_{sg}. \tag{8}$$

The adsorbed gas content V_{sg} is expressed as follows:

$$V_{sg} = \frac{V_L p}{p + p_L} \exp\left[-\frac{c_2}{1 + c_1 p}\left(T_{ar} + T - T_t\right)\right]. \tag{9}$$

According to the ideal gas law, we have

$$\rho_g = \frac{M_g}{R(T_{ar} + T)} p. \tag{10}$$

According to Equation (10), the gas density ρ_{ga} in the standard state is expressed as follows:

$$\rho_{ga} = \frac{M_g p_a}{R_a T_a}. \tag{11}$$

Considering that the gas in the coal rock is in the non-Darcy flow state, and according to the Forchheimer equation, the gas flow is expressed as follows:

$$-\nabla p = \frac{k_e}{\mu} \mathbf{v}_g + \frac{c_f \rho_g}{\sqrt{k}} \mathbf{v}_g \left|\mathbf{v}_g\right|, \tag{12}$$

where $c_f = 1.75/\sqrt{150\varepsilon^3}$ and ε is the porosity of coal rocks.

When the gas is in the Darcy flow state, the gas flow is expressed as follows:

$$\mathbf{v}_g = -\delta \frac{k_e}{\mu} \nabla p, \tag{13}$$

where $\delta = 1/(1 + (\sqrt{k_e}/\mu) c_f \rho_g |\mathbf{v}_g|)$.

Generally, the relation of porosity between mean stress and pressure is expressed as follows:

$$d\phi = \frac{1}{K}(\alpha - \phi)(d\bar{\sigma} + dp). \tag{14}$$

Integrating both sides of Equation (13), we get

$$\int_{\phi_0}^{\phi} \frac{d\phi}{\alpha - \phi} = \frac{1}{K}\left(\int_{\bar{\sigma}_0}^{\bar{\sigma}} d\bar{\sigma} + \int_{p_0}^{p} dp\right), \tag{15}$$

$$\phi = \alpha - (\alpha - \phi_0) \exp\left\{-\frac{1}{K}[(\bar{\sigma} - \bar{\sigma}_0) + (p - p_0)]\right\}. \tag{16}$$

The subscript 0 indicates the initial state of the parameter. Substituting Equation (4) into Equation (16), we get

$$\phi = \alpha - (\alpha - \phi_0) \exp\left\{-\left[\left(\varepsilon_V + \frac{p}{K_s} - \varepsilon_s - \alpha_T T\right) - \left(\varepsilon_{V0} + \frac{p_0}{K_{s0}} - \varepsilon_{s0} - \alpha_T T_0\right)\right]\right\}. \tag{17}$$

According to the Klinkenberg slippage effect during gas flow, the effective gas permeability is related to pressure, and their relationship is expressed as follows:

$$k_e = k_\infty \left(1 + \frac{b}{p_f}\right). \tag{18}$$

k_∞ is the absolute permeability under the very high pore pressure, and the Klinkenberg slippage is negligible; b is the Klinkenberg factor related to the mean free path of gas molecules, and the mean free path depends on temperature, pore pressure, and gas molar mass. The Klinkenberg factor is expressed as follows:

$$b = \alpha_k k_\infty^{-0.36}. \tag{19}$$

According to the experimental estimation, $\alpha_k = 0.251$.

The relationship between gas permeability and porosity is expressed as follows:

$$k_e = k_{\infty 0}\left(1 + \frac{b}{p_f}\right)\left(\frac{\phi}{\phi_0}\right)^3. \tag{20}$$

By substituting Equations (8) to (20) into Equation (7), we get [14]

$$\frac{\partial \phi}{\partial t}\frac{1}{T_{ar} + T} p + \phi \frac{1}{T_{ar} + T}\frac{\partial p}{\partial t} - \phi p \frac{1}{(T_{ar} + T)^2}\frac{\partial T}{\partial t} + \frac{p_a \rho_c V_L}{T_a}\left\{\begin{array}{c} \dfrac{p_L}{(p + p_L)^2} \exp\left(-\dfrac{c_2}{1 + c_1 p}(T + T_{ar} - T_t)\right)\dfrac{\partial p}{\partial t} \\ + \dfrac{p}{p + p_L} \exp\left(-\dfrac{c_2}{1 + c_1 p}(T + T_{ar} - T_t)\right) \times \dfrac{c_1 c_2}{(1 + c_1 p)^2}(T + T_{ar} - T_t)\dfrac{\partial p}{\partial t} \\ - \dfrac{p}{p + p_L} \exp\left(-\dfrac{c_2}{1 + c_1 p}(T + T_{ar} - T_t)\right) \times \dfrac{c_2}{1 + c_1 p}\dfrac{\partial T}{\partial t} \end{array}\right\}$$
$$- \frac{1}{\mu}\left[\frac{\partial}{\partial x}\left(\frac{\delta p k_e}{T_{ar} + T}\frac{\partial p}{\partial x}\right) + \frac{\partial}{\partial y}\left(\frac{\delta p k_e}{T_{ar} + T}\frac{\partial p}{\partial y}\right)\right] = Q_s. \tag{21}$$

3.3. Energy Conservation Equation. When the heat carried out by the gas flow is ignored, the total heat flux density is expressed as follows:

$$q_T = -\lambda_M \nabla T + \rho_g C_g q_g (T_{ar} + T), \tag{22}$$

where $\lambda_M = (1 - \phi)\lambda_s + \phi \lambda_g$.

When the mutual conversion between thermal energy and mechanical energy is ignored, the thermal balance equation is expressed as follows:

$$\frac{\partial\left[(\rho C)_M (T_{ar} + T)\right]}{\partial t} + (T_{ar} + T) K_g \alpha_g \nabla \cdot \left(\frac{k_e}{\mu}\nabla p\right) + (T_{ar} + T) K \alpha_T \frac{\partial \varepsilon_V}{\partial t} = -\nabla \cdot q_T, \tag{23}$$

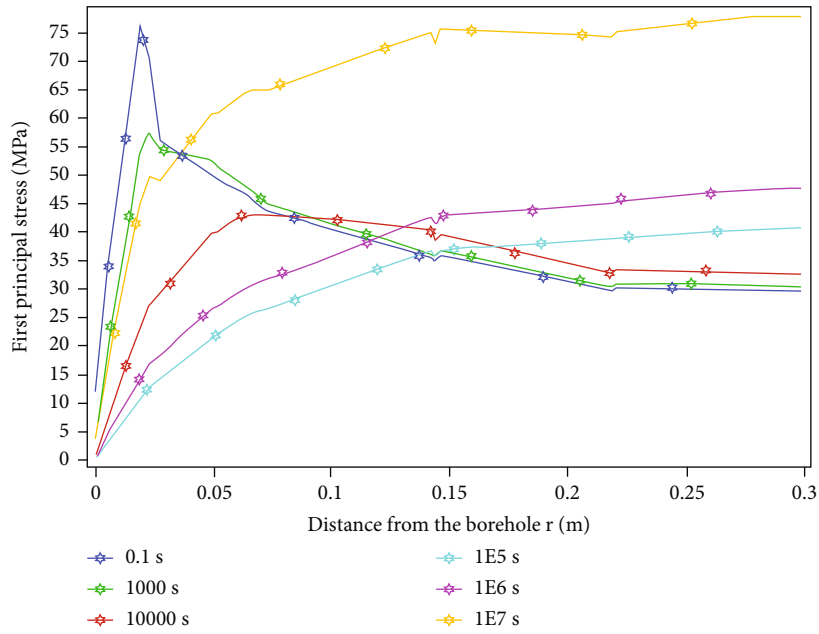

Figure 5: First principal stress in the homogeneous coal rock during CBM production.

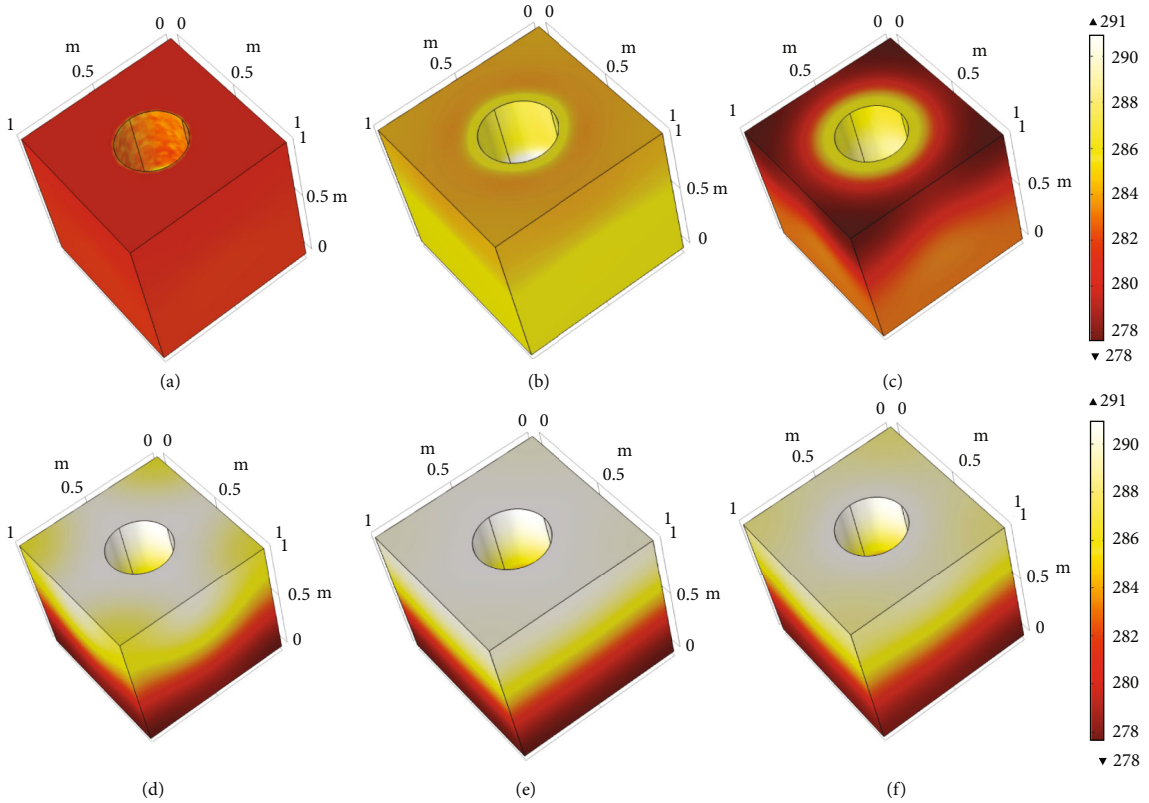

Figure 6: Thermal field in the homogeneous coal rock: (a) $t = 0.1$ s, (b) $t = 1 \times 10^3$ s, (c) $t = 1 \times 10^4$ s, (d) $t = 1 \times 10^5$ s, (e) $t = 1 \times 10^6$ s, and (f) $t = 1 \times 10^7$ s.

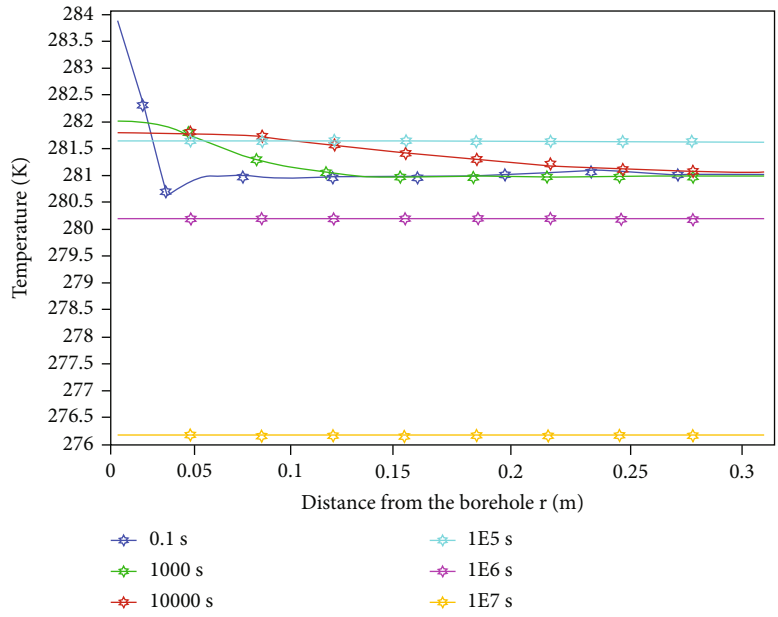

Figure 7: Temperature in the homogeneous coal rock during CBM production.

where $(\rho C)_M = \phi(\rho_g C_g) + (1-\phi)(\rho_s C_s)$, $\alpha_g = 1/T$, and $K_g = p$.

According to the law of mass conservation of matrix and gas in the coal rock, we have

$$\frac{\partial[(1-\phi)\rho_s]}{\partial t} = 0, \tag{24}$$

$$\frac{\partial\left(\phi\rho_g\right)}{\partial t} = -\nabla\cdot\left(\rho_g q_g\right). \tag{25}$$

$(1-\phi)\lambda_s >> \phi\lambda_s$ and $\lambda_M \approx (1-\phi)\lambda_s \approx \lambda_s$; Equation (23) is transferred to [14]

$$(\rho C)_M \frac{\partial T}{\partial t} - (T_{ar}+T)K_g\alpha_g\nabla\cdot\left(\frac{k_e}{\mu}\nabla p\right) + (T_{ar}+T)K\alpha_T\frac{\partial\varepsilon_V}{\partial t} = \lambda_M\nabla^2 T + \frac{\rho_{ga}pT_a C_g}{p_a(T_{ar}+T)}\frac{k_e}{\mu}\nabla p\nabla T. \tag{26}$$

It is the partial differential equation of the thermal field in the coal rock.

3.4. Mechanical Heterogeneity Characterization. According to the previous scholars' experience, Weibull's function can better describe the mechanical heterogeneity of porous media, which is in line with reality compared to other random functions. Weibull's probability density distribution function is a method to characterize the rock heterogeneity, which is realized by constraint of the rock physical parameters with the Weibull distribution and random assignment of physical parameters with the Monte Carlo method [11, 18]. Weibull's probability density function is expressed as follows:

$$f(x,m,n) = \begin{cases} \frac{m}{n}\left(\frac{x}{n}\right)^{m-1}\exp\left[-\left(\frac{x}{n}\right)^m\right], & x \geq 0, \\ 0, & x < 0. \end{cases} \tag{27}$$

The smaller value of m indicates stronger heterogeneity. Here, the random distribution of the coal rock elastic modulus is considered. Figure 2 illustrates the 3D distribution of the elastic modulus in the RVE and the contour map at different planes. Heterogeneity degree $m = 7$, and the average elastic modulus $n = 1.85$ GPa.

3.5. Model Verification. According to the rock mechanics, there is an analytical solution to the stress field around the borehole in the homogeneous formation. The basic parameters are listed in Table 1. The analytical solutions and finite element numerical solutions to theS_{xx}component in the stress field are shown when the bottom hole pressure is 30 MPa, 40 MPa, and 50 MPa [22–24], respectively (Figure 3). The solutions have a high degree of agreement, which verifies the reliability of the finite element numerical solution under the HM coupling conditions.

4. Results and Discussion

The parameters of the finite element model are listed in Table 1. The 3D stress field, thermal field, and pressure field are obtained by simulating the THM coupling process in the homogeneous coal rock and the coal rock with the heterogeneity degree $m = 7$, 5, 3, and 1. The variation in the porosity

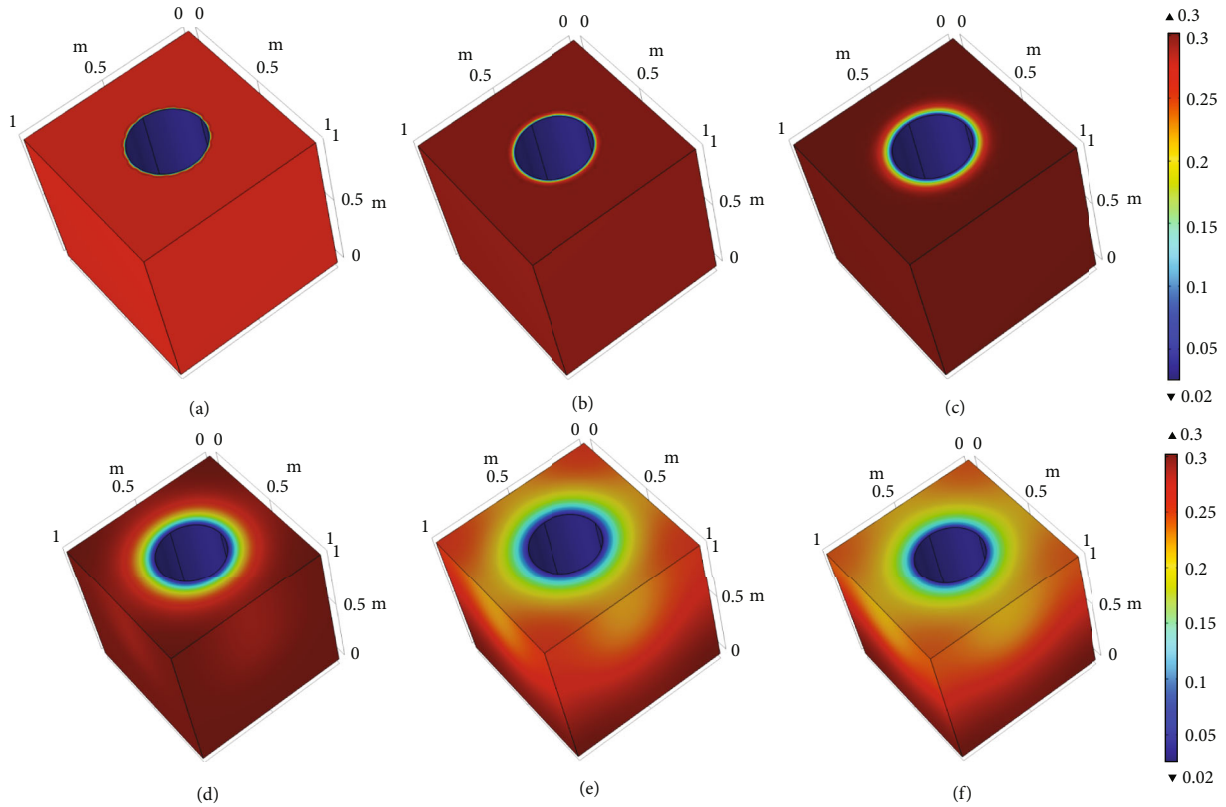

Figure 8: Pore pressure in the homogeneous coal rock: (a) $t = 0.1$ s, (b) $t = 1 \times 10^3$ s, (c) $t = 1 \times 10^4$ s, (d) $t = 1 \times 10^5$ s, (e) $t = 1 \times 10^6$ s, and (f) $t = 1 \times 10^7$ s.

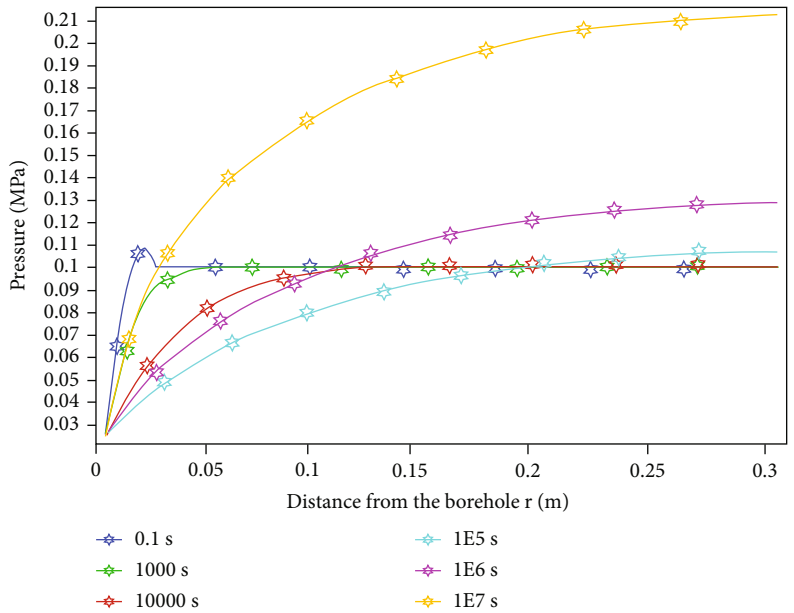

Figure 9: Pore pressure in the homogeneous coal rock during CBM production.

and permeability around the borehole with time and distance from the borehole under different conditions is analyzed.

4.1. Homogeneous Coal Rock. The 3D field of the first principal stress σ_H in the homogeneous coal rock REV is obtained (Figure 4). The principal stress is relatively higher

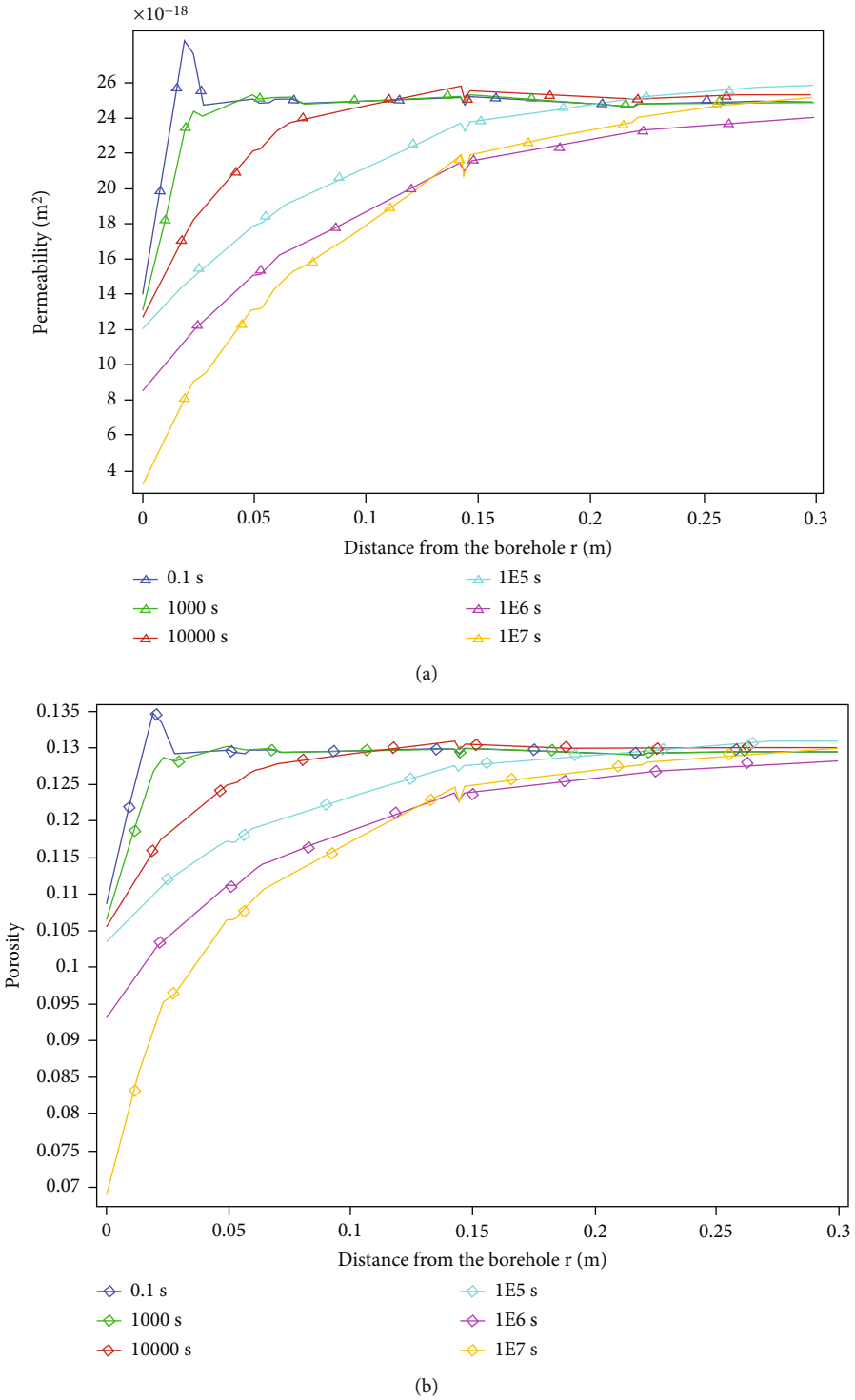

Figure 10: Gas permeability (a) and porosity (b) in the homogeneous coal rock during CBM production.

around the borehole, indicating stress concentration. The stress concentration spreads from the borehole to the coal rock as the CBM is produced. Figure 5 shows the first principal stress in the coal rock during CBM production. When the production time $t < 1 \times 10^4$ s, σ_H shows a downward trend during CBM production. As the distance from the borehole r increases, σ_H firstly increases and reaches a peak and then decreases to a stable value. When $t \geq 1 \times 10^4$ s, σ_H shows an upward trend during CBM production, and σ_H increases as r increases. When $r \geq 1.5$ m, σ_H is

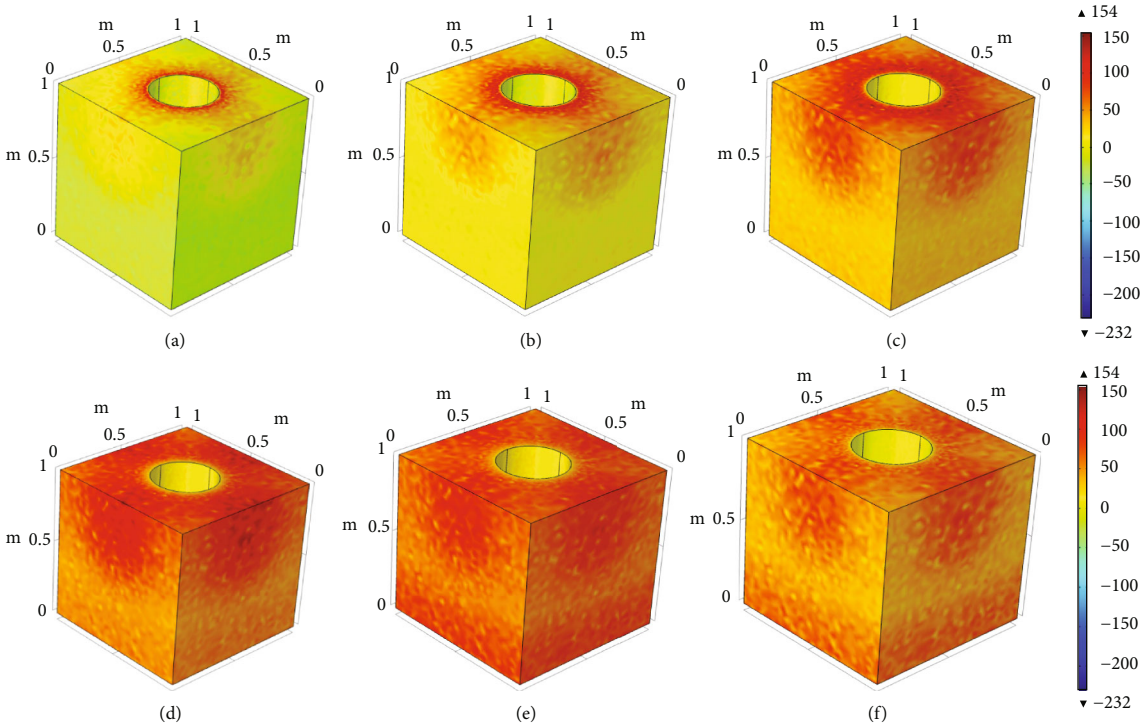

Figure 11: Stress field in the $m = 7$ coal rock: (a) $t = 0.1$ s, (b) $t = 1 \times 10^3$ s, (c) $t = 1 \times 10^4$ s, (d) $t = 1 \times 10^5$ s, (e) $t = 1 \times 10^6$ s, and (f) $t = 1 \times 10^7$ s.

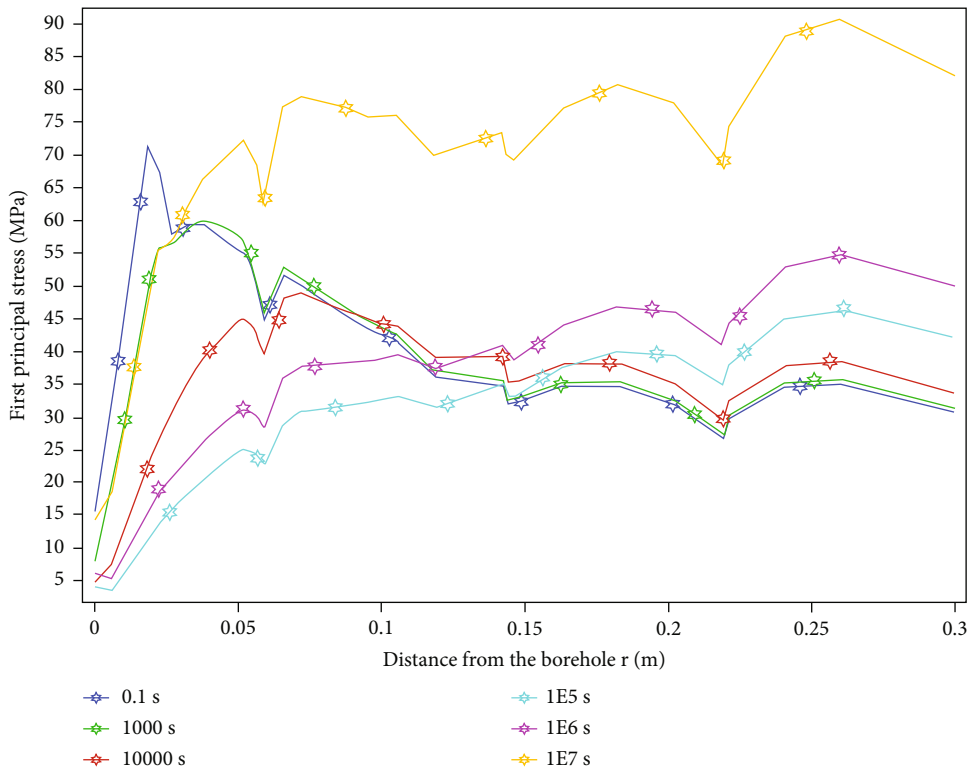

Figure 12: First principal stress in the $m = 7$ coal rock during CBM production.

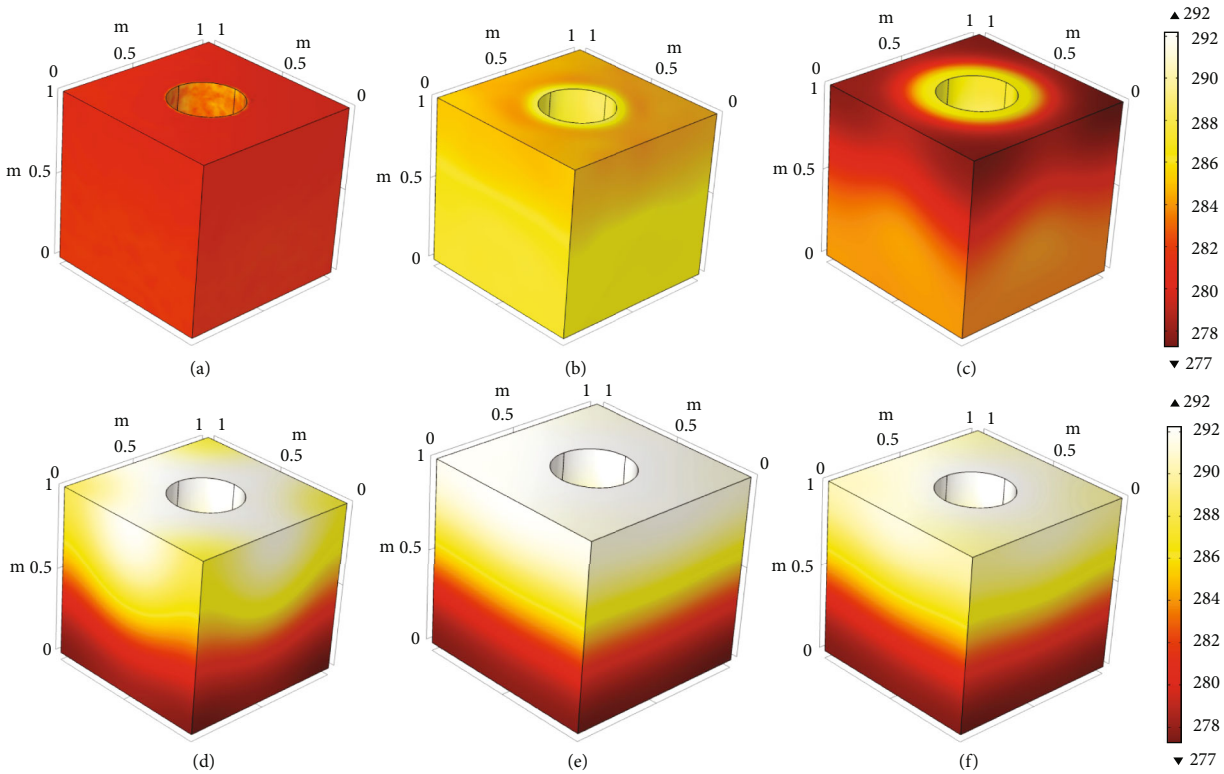

Figure 13: Thermal field in the $m = 7$ coal rock: (a) $t = 0.1$ s, (b) $t = 1 \times 10^3$ s, (c) $t = 1 \times 10^4$ s, (d) $t = 1 \times 10^5$ s, (e) $t = 1 \times 10^6$ s, and (f) $t = 1 \times 10^7$ s.

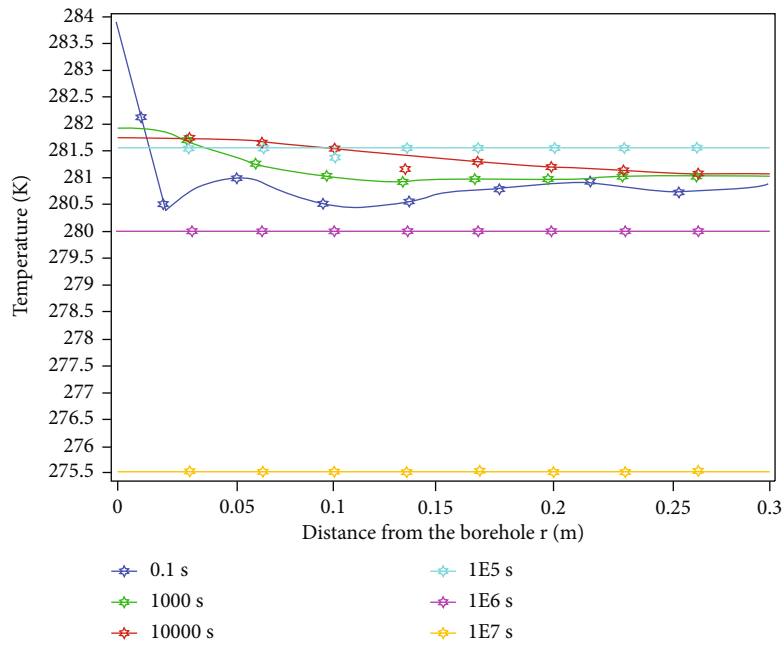

Figure 14: Temperature in the $m = 7$ coal rock during CBM production.

stabilized. σ_H varies significantly around the borehole, and its increment slows down when $r \geq 0.1$ m, which is caused by stress concentration.

The 3D thermal field in the homogeneous coal rock REV is obtained (Figure 6). As the CBM is produced, the temperature decreases gradually around the borehole, which is

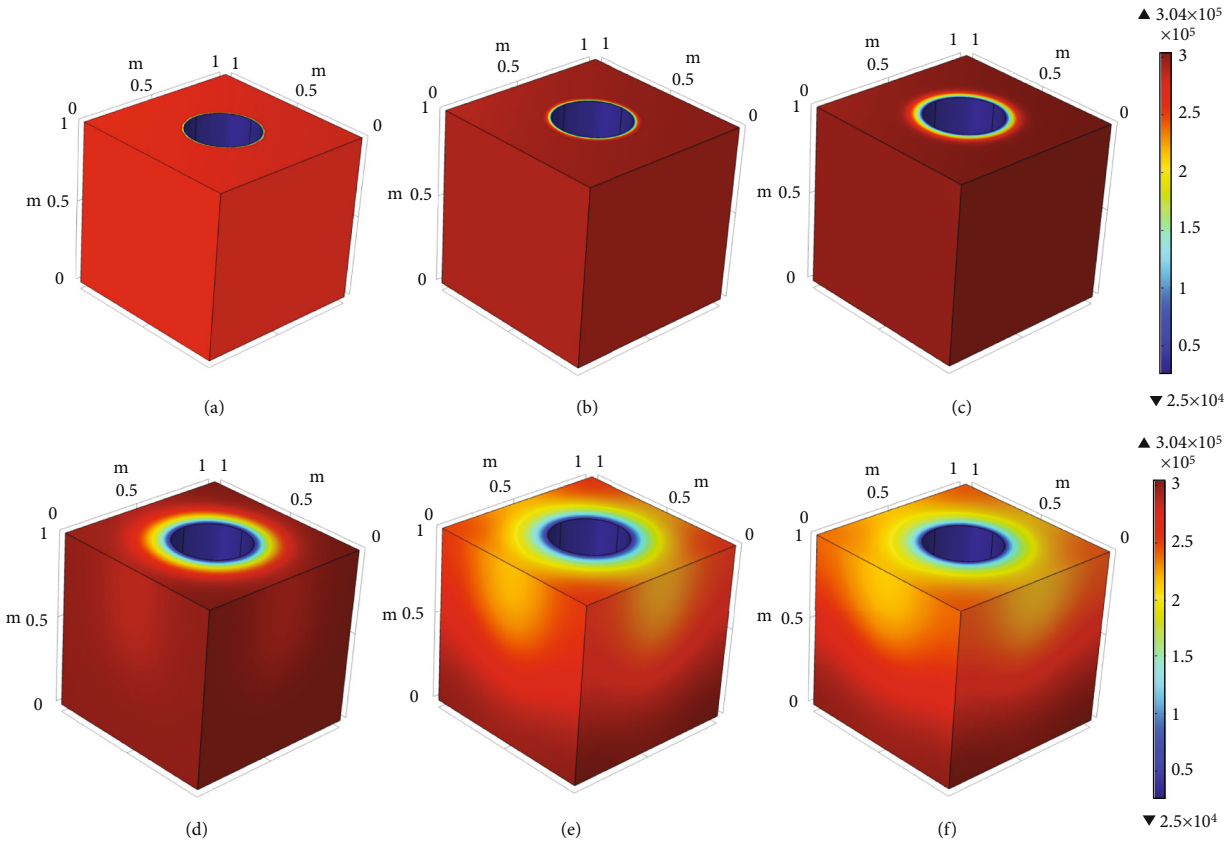

Figure 15: Pore pressure field in the $m = 7$ coal rock: (a) $t = 0.1$ s, (b) $t = 1 \times 10^3$ s, (c) $t = 1 \times 10^4$ s, (d) $t = 1 \times 10^5$ s, (e) $t = 1 \times 10^6$ s, and (f) $t = 1 \times 10^7$ s.

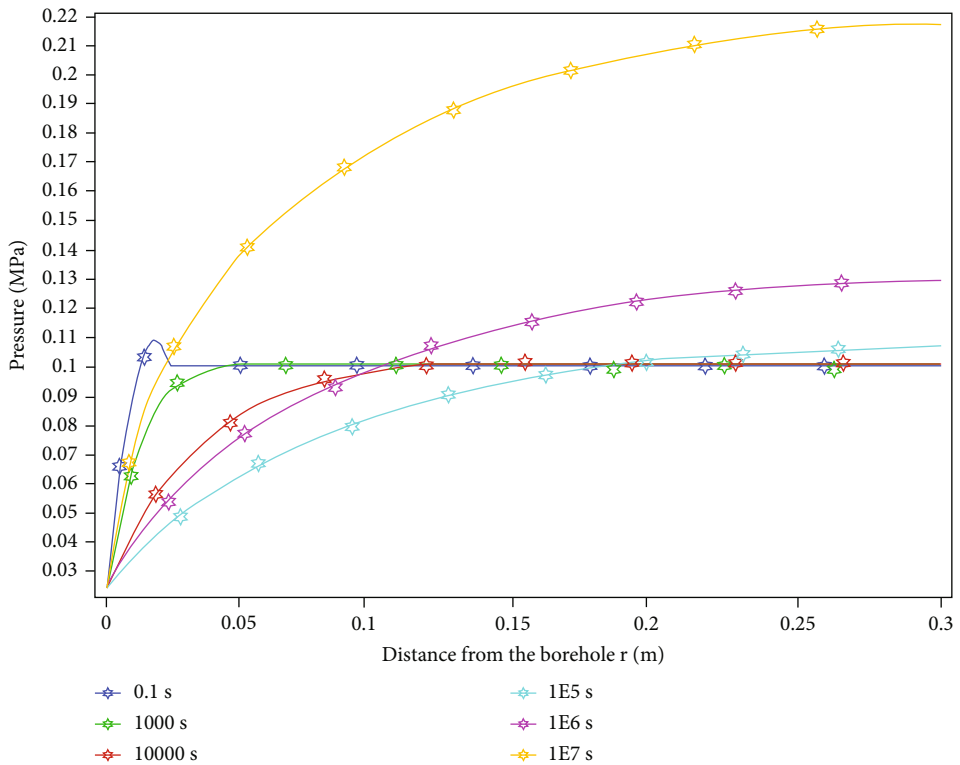

Figure 16: Pore pressure in the $m = 7$ coal rock during CBM production.

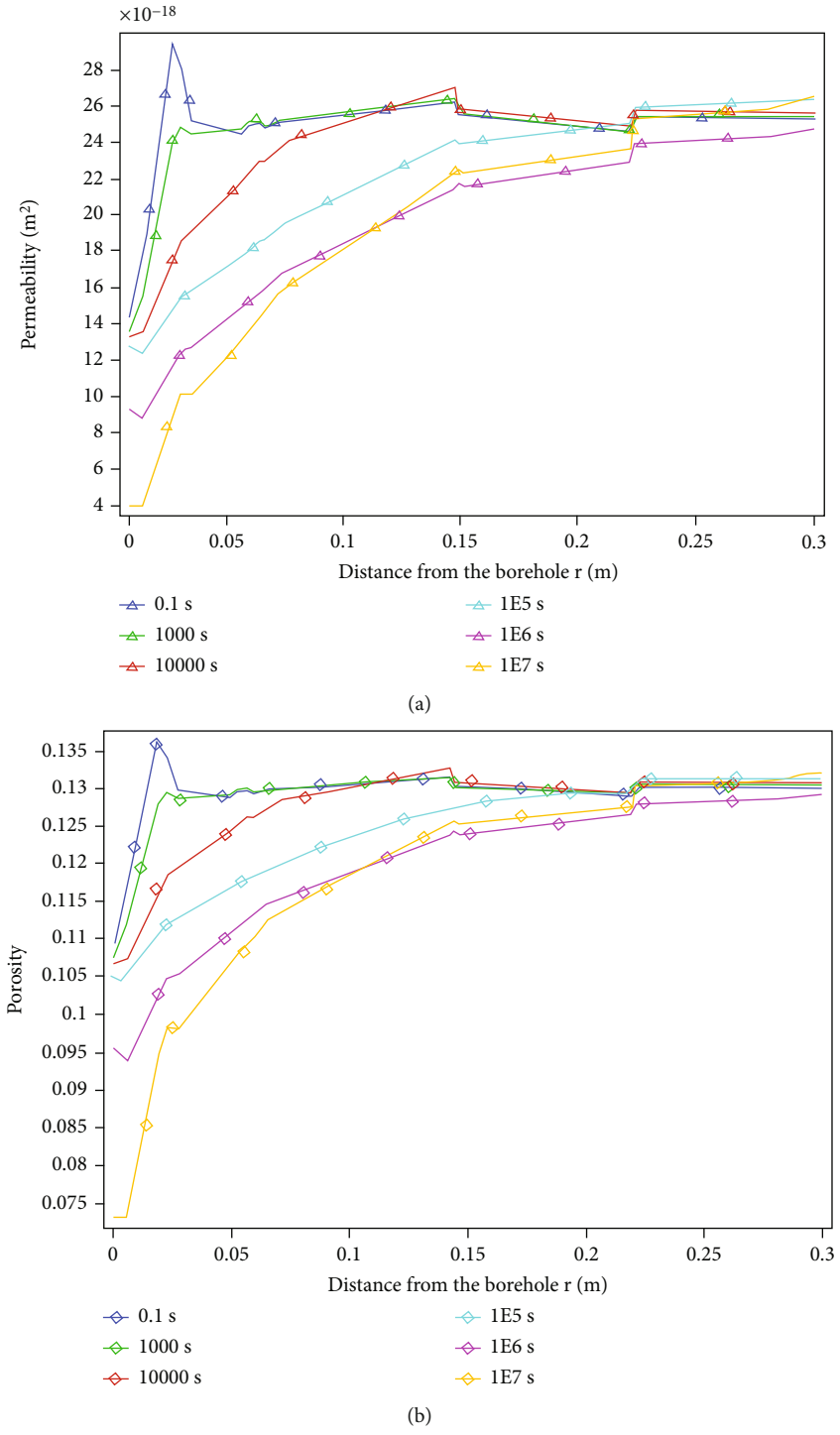

Figure 17: Permeability (a) and porosity (b) in the $m = 7$ coal rock during CBM production.

caused by methane adsorption and desorption, and the change in the thermal field spreads out. The temperature of the coal rock during CBM production is shown in Figure 7. The temperature rises as r increases, indicating that CBM production leads to cooling down around the borehole. When $t \geq 1 \times 10^4$ s, the thermal field in the coal rock is not changed.

The 3D pore pressure field in the homogeneous coal rock REV is obtained (Figure 8). The pore pressure field shows a circular distribution around the borehole. As the CBM is produced, the pressure wave gradually spreads out from the borehole. The pore pressure in the coal rock during CBM production is shown in Figure 9. As r increases, the pressure gradually increases, indicating that production

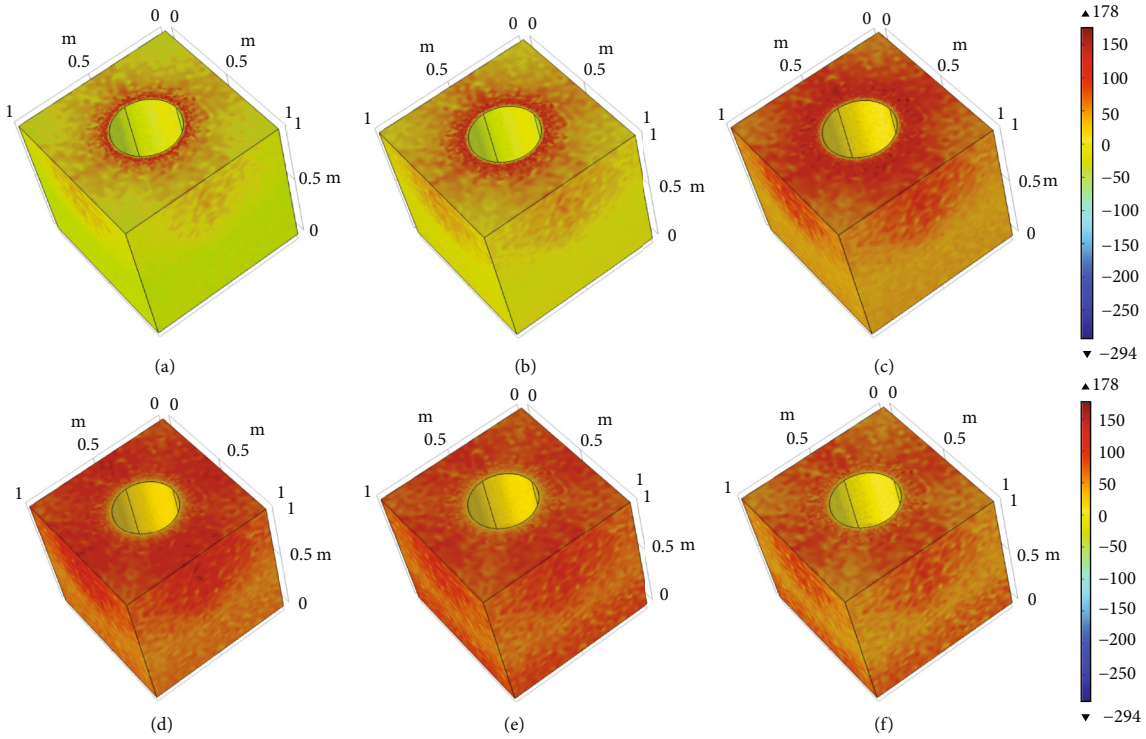

Figure 18: Stress field in the $m = 5$ coal rock: (a) $t = 0.1$ s, (b) $t = 1 \times 10^3$ s, (c) $t = 1 \times 10^4$ s, (d) $t = 1 \times 10^5$ s, (e) $t = 1 \times 10^6$ s, and (f) $t = 1 \times 10^7$ s.

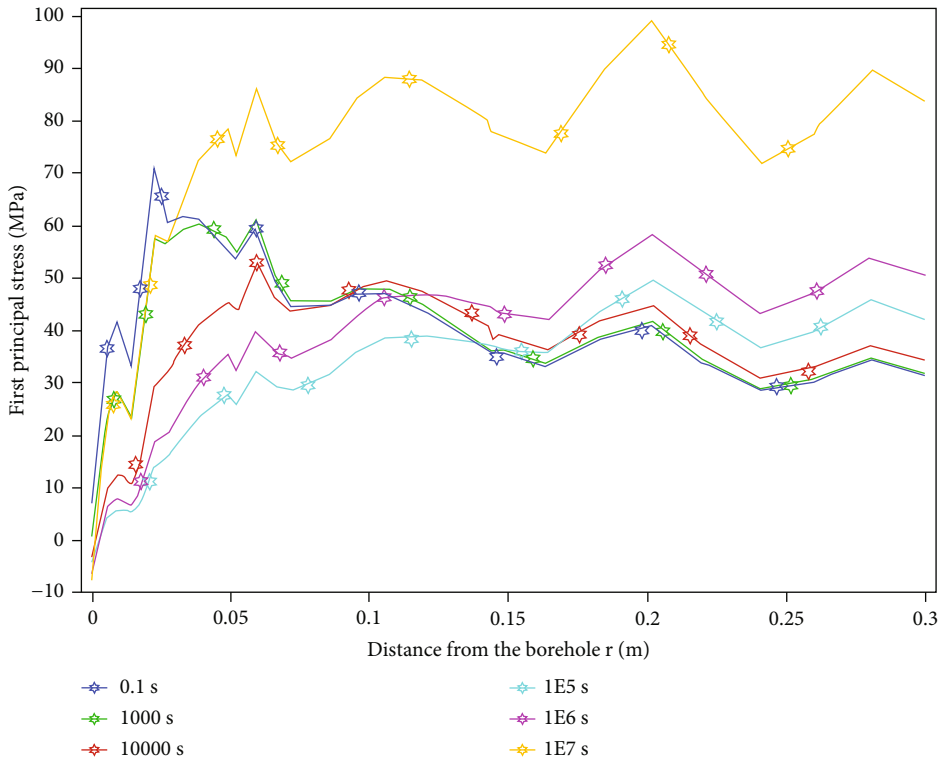

Figure 19: First principal stress in the $m = 5$ coal rock during CBM production.

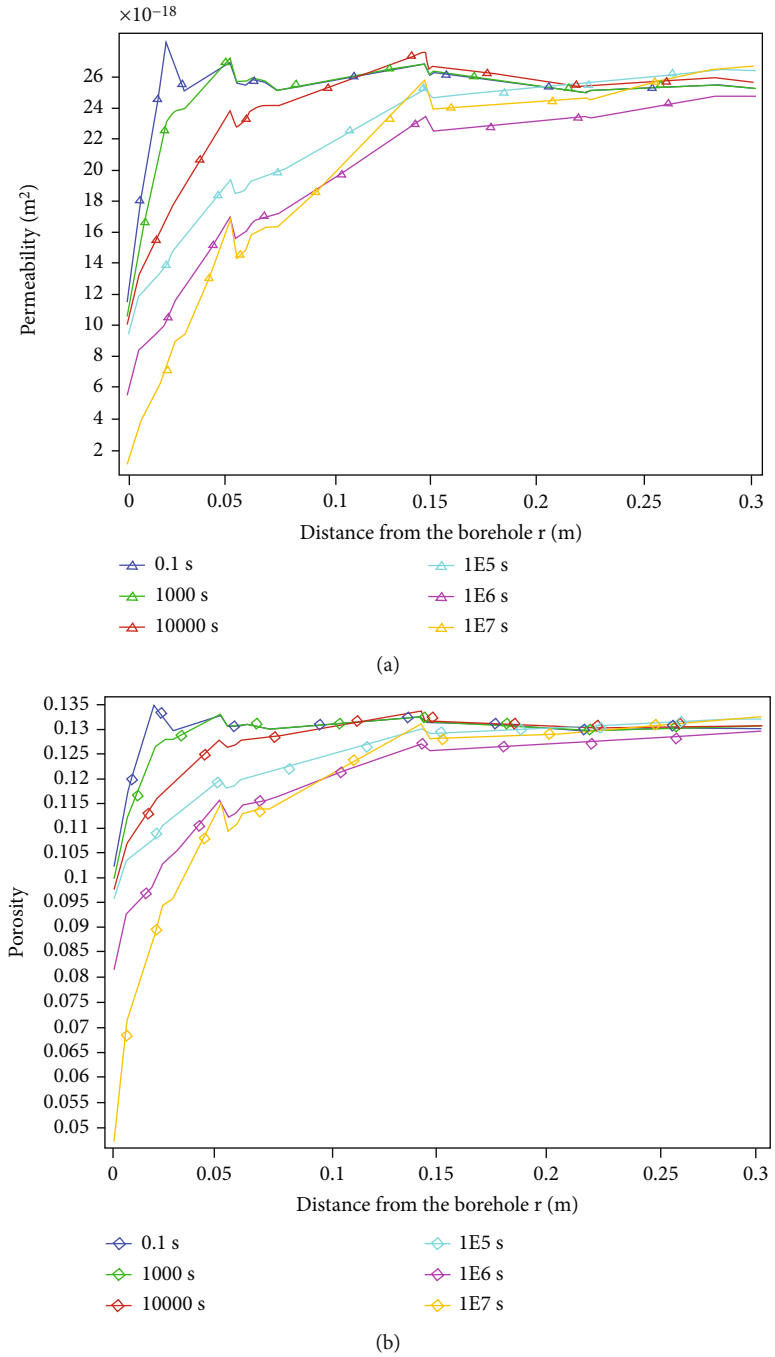

Figure 20: (a) Permeability and (b) porosity in the $m = 5$ coal rock during CBM production.

causes pressure depletion around the borehole. When $t \geq 1 \times 10^5$ s, the pore pressure shows a downward trend; when $t < 1 \times 10^5$ s, the pore pressure shows an upward trend.

The permeability and porosity in the coal rock with the homogeneous elastic modulus during CBM production are obtained (Figure 10). As the CBM is produced, the permeability and porosity decrease around the borehole. In the early production stage, the permeability and porosity decline faster. When $t \geq 1 \times 10^6$ s, the decrease slows down. The coal rock permeability and porosity decrease as r increases. In the area within 0.15 m of the borehole, the permeability and porosity decrease slower when $r \leq 0.15$ m and decrease faster when $r > 0.15$ m.

4.2. Heterogeneous Strata

4.2.1. Heterogeneous Coal Rock

(1) Heterogeneity Degree $m = 7$. The 3D principal stress field (Figure 11) around the borehole in the $m = 7$ coal rock shows the random distribution, which is caused by elastic

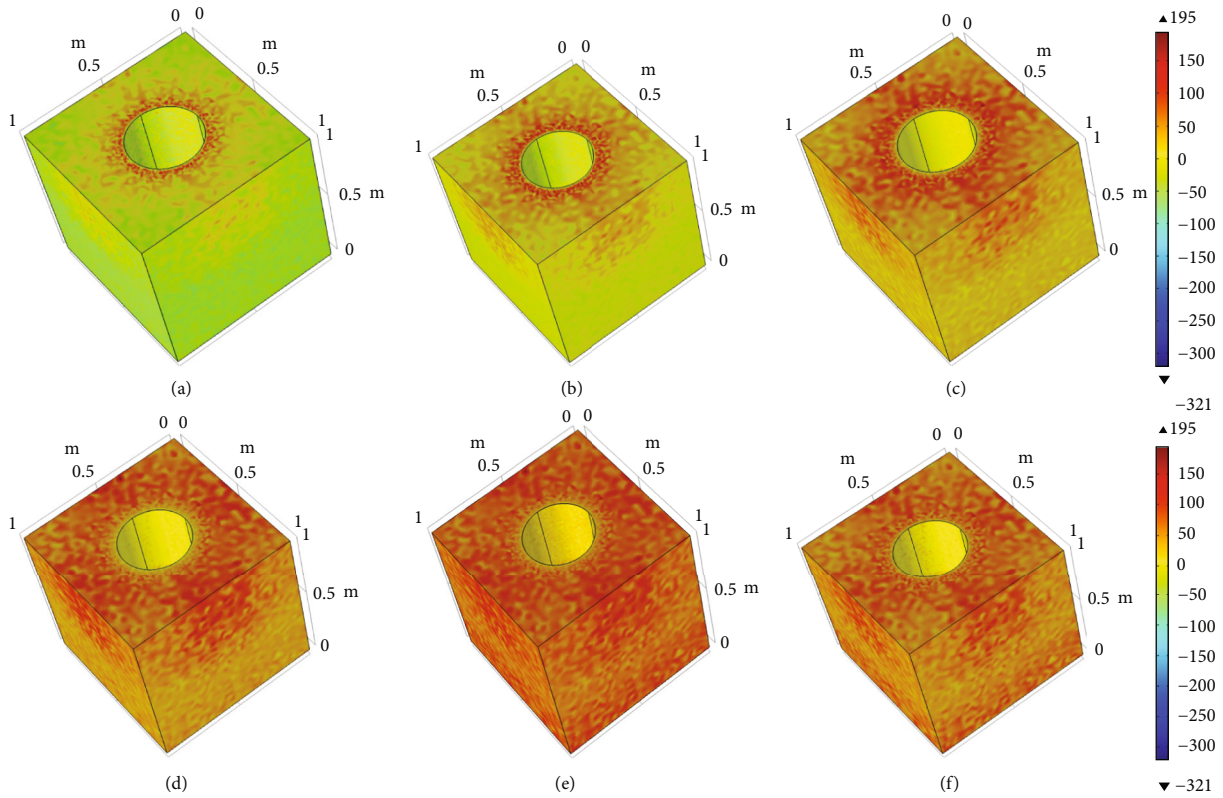

Figure 21: Stress field in the $m = 3$ coal rock: (a) $t = 0.1$ s, (b) $t = 1 \times 10^3$ s, (c) $t = 1 \times 10^4$ s, (d) $t = 1 \times 10^5$ s, (e) $t = 1 \times 10^6$ s, and (f) $t = 1 \times 10^7$ s.

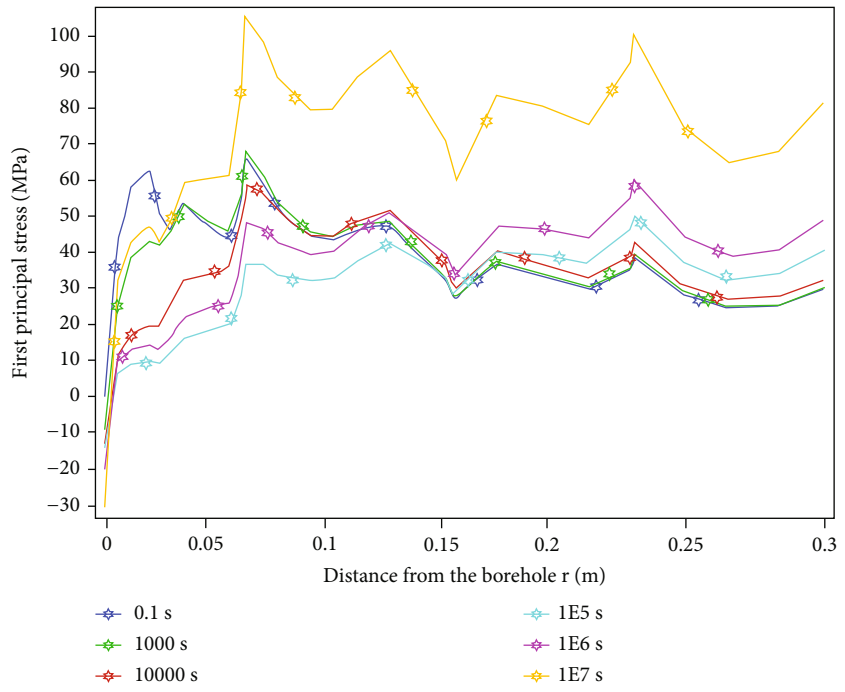

Figure 22: First principal stress in the $m = 3$ coal rock during CBM production.

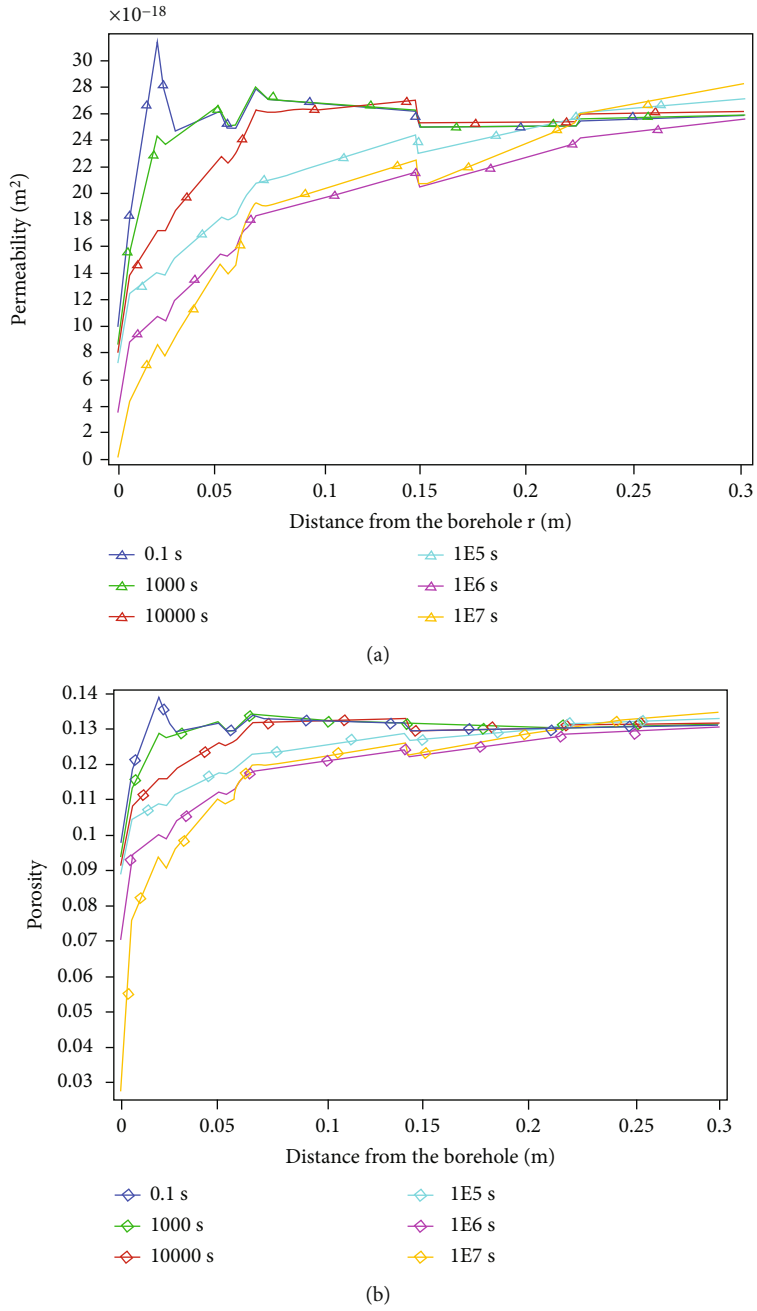

Figure 23: (a) Gas permeability and (b) porosity in the $m = 3$ coal rock during CBM production.

modulus heterogeneity. As the CBM is produced, the variation in the principal stress spreads out. Initially, the principal stress variation area is concentrated around the borehole. When $t \geq 1 \times 10^4$ s, the variation in σ_H spreads over the entire heterogeneous coal rock REV. The heterogeneity of the stress field is transmitted from the top to the bottom. Figure 12 shows the σ_H during CBM production. σ_H fluctuates as r the distance from the borehole increases. When $t < 1 \times 10^4$ s, σ_H decreases as the CBM is produced, which is similar to the phenomenon in the homogeneous coal rock (Figure 5). σ_H is relatively high around the borehole and is stabilized as r increases. When $t \geq 1 \times 10^4$ s, σ_H increases during CBM production. σ_H increases as r increases. When $r \geq 0.1$ m, σ_H fluctuates around a stable value, which is caused by mechanical heterogeneity.

Figure 13 shows the 3D thermal field in the $m = 7$ coal rock during CBM production. In the initial production stage, the temperature near the borehole shows a random distribution. When $t \geq 10^3$ s, the temperature is uniform over the coal rock REV. As production goes on, the variation in the thermal field gradually spreads out. Compared with the

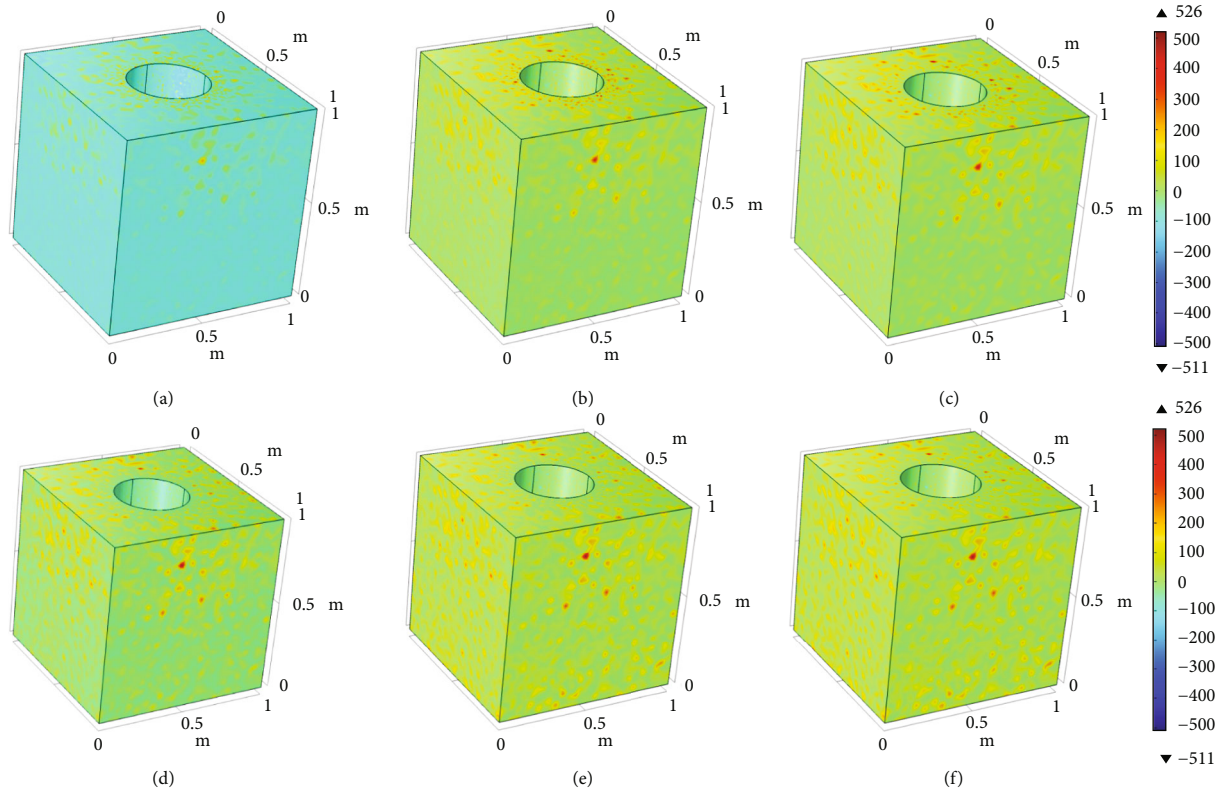

Figure 24: Stress field in the $m = 1$ coal rock: (a) $t = 0.1$ s, (b) $t = 1 \times 10^3$ s, (c) $t = 1 \times 10^4$ s, (d) $t = 1 \times 10^5$ s, (e) $t = 1 \times 10^6$ s, and (f) $t = 4.03 \times 10^6$ s.

stress field, the thermal field does not show obvious heterogeneity. This is because only the elastic modulus heterogeneity closely related to the stress field is considered in this study, and it has little effect on the thermal field. Figure 14 shows the temperature in the $m = 7$ coal rock during CBM production, which is the same as that in the homogeneous coal rock. The weak mechanical heterogeneity has little effect on the coal rock thermal field.

Figure 15 shows the 3D pore pressure field in the $m = 7$ coal rock during CBM production. The pore pressure field around the borehole shows the circular distribution. As CBM production goes on, the pressure wave gradually spreads out. When $t \geq 1 \times 10^6$ s, the pressure wave is stabilized and spreads from the top to the bottom of the REV, which is similar to the phenomenon in the homogeneous coal rock. Pressure heterogeneity propagation is not observed. This is because only the elastic modulus heterogeneity is considered and it has little effect on the pore pressure field. The pore pressure during CBM production is shown in Figure 16, which is the same as Figure 9. The weak mechanical heterogeneity has little effect on the coal rock pressure field. Another reason is that we do not consider the heterogeneous parameters of pore pressure equations in this paper. The mechanical heterogeneity of elastic modulus of coal rock has a negligible effect of pore pressure distribution despite the existence of multiple field coupling process.

The permeability and porosity in the coal rock with heterogeneous elastic modulus are obtained (Figure 17). The permeability and porosity in the heterogeneous coal rock fluctuate and vary as r increases. As CBM production goes on, the permeability and porosity of the coal rock show a downward trend.

(2) Heterogeneity Degree $m = 5$. The principal stress field in the $m = 5$ coal rock shows the random distribution (Figure 18). σ_H when $m = 5$ is higher than that when $m = 7$. The reason is that stronger mechanical heterogeneity causes local stress concentration and an increase in principal stress. As CBM production goes on, the variation in the stress field gradually spreads out. Initially, the stress only varies around the borehole. When $t \geq 1 \times 10^4$ s, the wave in the stress field spreads over the coal rock REV. The stress field heterogeneity is transmitted from the top to the bottom of the REV. σ_H in the $m = 5$ coal rock during CBM production is shown in Figure 19. σ_H fluctuates as r increases, which is the same as the phenomenon when $m = 7$. Compared with that when $m = 7$, σ_H when $m = 5$ fluctuates more frequently, which is caused by stronger mechanical heterogeneity.

When $m = 5$, the gas permeability and porosity fluctuate as r increases (Figure 20). As CBM production goes on, both

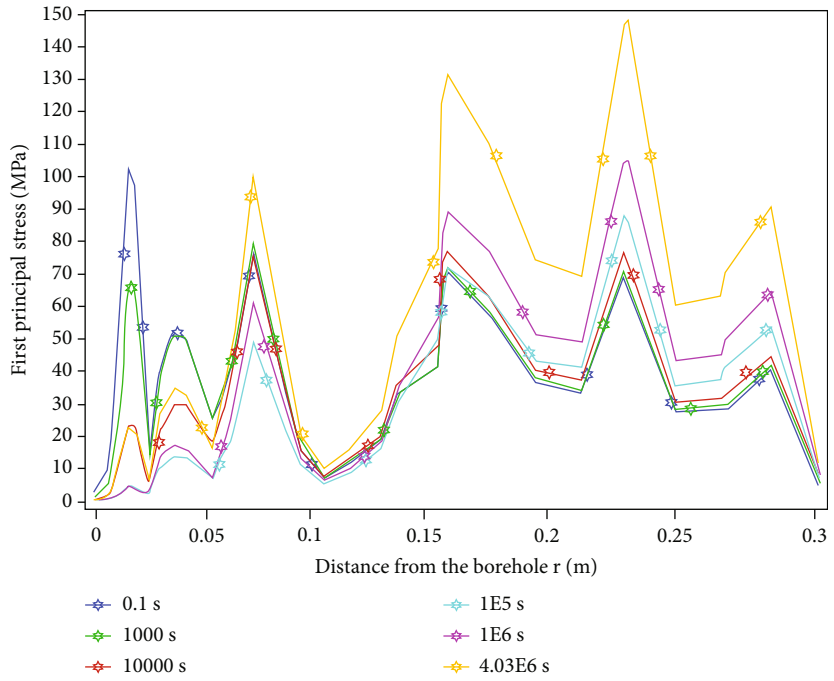

Figure 25: First principal stress in the $m = 1$ coal rock during CBM production.

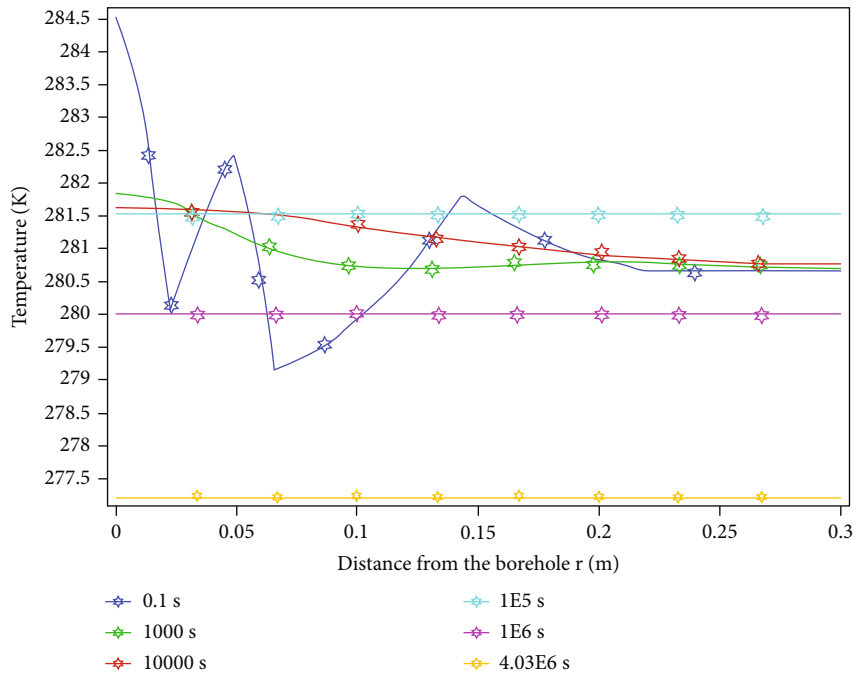

Figure 26: Temperature in the $m = 1$ coal rock during CBM production.

gas permeability and porosity show a downward trend. Moreover, they fluctuate more frequently, which is caused by stronger heterogeneity.

(3) Heterogeneity Degree $m = 3$. When $m = 3$, the first principal stress field shows the random distribution around the borehole (Figure 21). σ_H when $m = 3$ is higher than that when $m = 7$. As CBM production goes on, the variation in the first principal stress gradually spreads out. Initially, σ_H only varies around the borehole. When $t \geq 1 \times 10^5$ s, the variation in the stress field spreads over the entire coal rock REV. The first principal stress in the $m = 3$ coal rock during

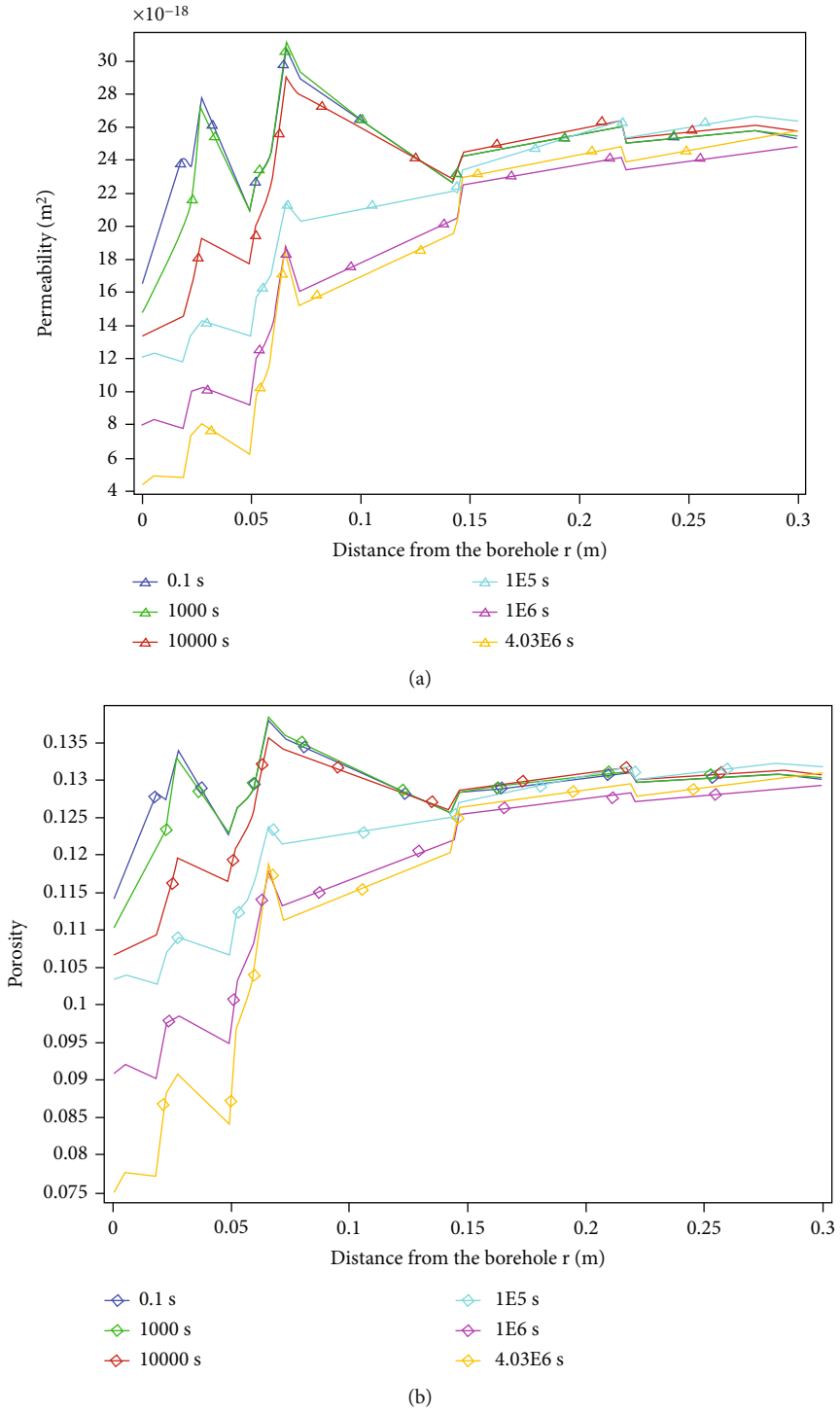

Figure 27: (a) Gas permeability and (b) porosity in the $m = 1$ coal rock during CBM production.

CBM production is obtained (Figure 22). As r increases, σ_H fluctuates even more frequently, which is caused by stronger mechanical heterogeneity.

When $m = 3$, the gas permeability and porosity fluctuate more frequently (Figure 23). As CBM production goes on, both gas permeability and porosity in the coal rock show a downward trend.

(4) Heterogeneity Degree $m = 1$. When $m = 1$, σ_H shows the random distribution around the borehole (Figure 24). Stronger mechanical heterogeneity leads to a higher value of σ_H.

As CBM production goes on, the variation in the stress area spreads out. When $t \geq 1 \times 10^6$ s, variation in σ_H spreads over the entire REV.

When $m = 1$, σ_H fluctuates most frequently (Figure 25). As r increases, the thermal field also fluctuates, which is caused by the THM coupling effect (Figure 26). When the mechanical heterogeneity is strong (high value of m), the effect of the mechanical heterogeneity on the thermal field is negligible.

When $m = 1$, the gas permeability and porosity fluctuate more frequently. As the CBM is produced, both permeability and porosity in the coal rock show a downward trend (Figure 27).

5. Discussions and Analysis

The computation cost is increased with the increase of the degree of heterogeneity. This is because the stiffness matrix is not symmetric at different levels of heterogeneous parameter m. With the increase of the degree of heterogeneity, the randomness of the stiffness matrix is enhanced, which leads to the extended computation time.

The 3D THM coupled model in this paper considers the complex process such as desorption and adsorption, thermal expansion, and pore pressure variation in heterogeneous coal rock. The mechanical heterogeneity of elastic modulus is incorporated into the THM model by Weibull's random function. However, the thermal parameters such as thermal conductivity and specific heat capacity are not considered in the THM model, which can be done as the next work. Besides, the coal cleats widely distribute in the coal body. Coal rock body is simplified as a double-medium model, including a plenty of micropores and cleats. A more complex THM model can be extended by considering the cleat deformation and thermal expansion in future.

6. Conclusions

We characterize the mechanical heterogeneity of the coal rock based on Weibull's probability density distribution function and establish a THM coupling 3D model in the finite element commercial software COMSOL by considering variation in the pore pressure caused by methane gas desorption and adsorption and rock deformation and thermal expansion effect. We carry out a numerical simulation on the temporal and spatial evolution of gas permeability and porosity through the correlation between gas permeability and porosity and the THM coupling effect. The conclusions are as follows:

(1) The mechanical heterogeneity of coal rock has a significant effect on gas permeability and porosity. Compared with homogeneous coal rock, the heterogeneous coal rock shows the fluctuating distribution of permeability and porosity. The porosity and permeability vary significantly in different positions of the coal rock.

(2) Similar to the homogeneous coal rock, the heterogeneous coal rock has decreasing permeability and porosity as CBM is produced. The time for variation in the first principal stress transmitted to whole coal rock REV is longer, and the first principal stress increases, because the mechanical heterogeneity enhances the local stress concentration in the coal rock.

(3) When the coal rock has weak heterogeneity, the effect of mechanical heterogeneity on the thermal field and pressure field is negligible. When the coal rock has strong heterogeneity, the mechanical heterogeneity causes fluctuation in the thermal field due to the THM coupling effects.

(4) The evolution of porosity and permeability in the heterogeneous coal rock is a complex THM coupling process, which is closely related to mechanical heterogeneity, thermal expansion effect, pressure change caused by methane gas desorption, and stressed deformation of coal rock skeleton.

(5) In CBM exploitation, we should pay attention to the effects of mechanical heterogeneity on the porosity and gas permeability which are key parameters affecting CBM production. The mechanical heterogeneity varies within the coal bed and leads to multiple orders of magnitudes of gas permeability under the THM coupling effect. Thus, exploitation techniques should be optimized in the coal bed with different gas permeability and porosity.

(6) The heterogeneity of thermal parameters such as thermal conductivity and specific heat capacity, rock porosity, and permeability on THM coupling process can be incorporated into the current model. In addition, the double-porosity THM model with consideration coal cleats can be developed on basis of the model in this paper.

Nomenclature

σ_{ij}: Stress tensor (MPa)
f_i: Volumetric force vector (MPa)
ε_{ij}: Strain tensor (dimensionless)
G: Shear modulus (MPa)
μ: Poisson's ratio (dimensionless)
p: Gas pressure (MPa)
α: Biot coefficient (dimensionless)
δ_{ij}: Kronecker delta symbol (dimensionless) and $\delta_{ij} = 1$ when $i = j$ and $\delta_{ij=}0$ when $i \neq j$
T: Temperature (K)
ε_s: Volumetric strain caused by adsorption (dimensionless)
α_T: Linear thermal expansion coefficient (1/K)
u_i: Displacement vector (m)
ε_V: Volumetric strain, $\varepsilon_V = \varepsilon_{11} + \varepsilon_{22} + \varepsilon_{33}$ (dimensionless)

$\bar{\sigma} = \sigma_{kk}/3$: Average stress (MPa)
σ_{eij}: Effective stress (MPa)
V_{sg}: Adsorbed gas content (m^3)
α_{sg}: Volumetric strain coefficient caused by gas adsorption ($1/m^3$)
m: Gas content (m^3)
t: Production time (s)
σ_H: The first principal stress (MPa)
r: Distance from the borehole center (m)
ρ_g: Gas density (kg/m^3)
v_g: Seepage velocity vector (m/s)
Q_s: Source term (m^3/s)
ϕ: Porosity (dimensionless)
ρ_{ga}: Gas density in the standard state (kg/m^3)
ρ_c: Coal rock density (kg/m^3)
V_L: Langmuir volume constant at a temperature of T_t (m^3)
p_L: Pressure constant at a temperature of T_t (MPa)
T_{ar}: Absolute reference temperature in the unstressed state (K)
T_t: Referenced temperature in the gas desorption test (K)
$T_{ar} + T$: Coal rock temperature (K)
c_1: Pressure coefficient (dimensionless)
c_2: Temperature coefficient (dimensionless)
M_g: Gas molecular mass (kg/mol)
R: Gas universal constant (J/(kg·K))
p_a: Gas pressure in the standard state (MPa)
T_a: Temperature in the standard state (K)
μ: Viscosity (mPa·s)
k_e: Gas permeability (m^2)
C_f: Drag coefficient (dimensionless)
δ: Darcy correction coefficient (dimensionless)
q_T: Thermal flux density ($J/(m^2 \cdot s)$)
C_g: Specific heat capacity of gas at constant volume (J/(kg·K))
Q_g: Darcy flow rate (m/s)
λ_M: Coal rock thermal conductivity (W/(m·K))
λ_s: Matrix thermal conductivity (W/(m·K))
λ_g: Gas thermal conductivity (W/(m·K))
x: Variables such as elastic modulus and permeability
m: Shape parameter (dimensionless)
n: Average of a random variable
exp: Exponential function (dimensionless)
$(\rho C)_M$: Specific heat capacity of the coal rock medium filled by gas (J/(kg·K))
ρ_s: Coal density (kg/m^3)
C_s: Specific heat capacity of the matrix at constant volume (J/(kg·K))
α_g: Gas thermal expansion coefficient at constant pressure (1/K).

Data Availability

Datasets related to this article can be found by contacting the corresponding author.

Conflicts of Interest

The authors declare that they have no conflict of interests.

Acknowledgments

This work was supported financially by the Beijing Natural Science Foundation Project (3222030), the National Natural Science Foundation of China (51936001 and 52174045), the PetroChina Science and Technology Innovation Foundation Project (2021DQ02-0201), and the Science and Technology Project of PetroChina Company Limited "Research on Effective Reservoir Prediction and High-efficiency Well Optimization Technology for Deep/Ultra-Deep Oil and Gas Reservoirs" (2021DJ1003).

References

[1] X. Yang, F. Xu, H. Wang et al., "Exploration and development process and enlightenment of coalbed methane in eastern margin of Ordos Basin," *Coal Geology & Exploration*, vol. 1, no. 1, pp. 1–13, 2022.

[2] S. Wang, Z. Xiong, S. Lv, and C. Gao, "Characteristics and significance of proppant in hydraulic fractures in coal reservoirs," *Coal Geology & Exploration*, vol. 1, no. 1, pp. 1–10, 2022.

[3] G. Ni, Z. Li, Y. Wen, H. Jiang, Y. Liu, and Q. Huang, "Evolution of coalbed methane output and reservoir permeability under CO2 injection," *Journal of Mining and Safety Engineering*, vol. 1, no. 1, pp. 1–10, 2022.

[4] Z. Feng, Z. Wang, Y. Zhao, G. Li, Y. Zhang, and C. Wang, "Experimental investigation into deformation characteristics of anthracite under thermo-mechanical coupling conditions," *Chinese Journal of Rock Mechanics and Engineering*, vol. 29, no. 8, pp. 1624–1630, 2010.

[5] G. Yin, C. Jiang, J. G. Wang, and J. Xu, "Combined effect of stress, pore pressure and temperature on methane permeability in anthracite coal: an experimental study," *Transport in Porous Media*, vol. 100, pp. 1–16, 2013.

[6] S. Liu, C. Wei, W. Zhu, and M. Zhang, "Temperature- and pressure-dependent gas diffusion in coal particles: numerical model and experiments," *Fuel*, vol. 266, p. 117054, 2020.

[7] Y. Cai, D. Liu, J. P. Mathews et al., "Permeability evolution in fractured coal — combining triaxial confinement with X-ray computed tomography, acoustic emission and ultrasonic techniques," *International Journal of Coal Geology*, vol. 122, pp. 91–104, 2014.

[8] J. Huang, Z. Song, Z. Liao, W. Zhao, and D. Wang, "Quantification of cracks and the evolution of permeability for reservoir rock under coupled THM: equipment development and experimental research," *Geomechanics and Geophysics for Geo-Energy and Geo-Resources*, vol. 6, no. 4, pp. 1–13, 2020.

[9] T. Yang, S. Chen, W. Zhu, H. Liu, Z. Huo, and W. Jiang, "Coupled model of gas-solid in the coal rocks based on dynamic process of pressure relief and gas drainage," *Rock and Soil Mechanics*, vol. 31, no. 7, pp. 2247–2252, 2010.

[10] Z. Ma, *Study on Numerical Simulation of Gas Drainage Base on Thermo-Hydro-Mechanical Coupling*, Anhui University of Science and Technology, China, 2014.

[11] C. Wei, *Damage Model for Coal Rock Under Coupled Thermal-Hydraulic-Mechanical Conditions and Its Application*, Northeastern University, United States, 2012.

[12] Y. Tao, J. Xu, D. Liu, and Y. Liang, "Development and validation of THM coupling model of methane-containing coal," *International Journal of Mining Science and Technology*, vol. 22, no. 6, pp. 879–883, 2012.

[13] L. J. Hosking, M. Chen, and H. R. Thomas, "Numerical analysis of dual porosity coupled thermo-hydro-mechanical behaviour during CO_2 sequestration in coal," *International Journal of Rock Mechanics and Mining Sciences*, vol. 135, article 104473, 2020.

[14] Y. Xue, F. Gao, Y. Gao, X. Liang, Z. Zhang, and Y. Xing, "Thermo-hydro-mechanical coupled mathematical model for controlling the pre-mining coal seam gas extraction with slotted boreholes," *International Journal of Mining Science and Technology*, vol. 27, no. 3, pp. 473–479, 2017.

[15] Y. Zhao, B. Lin, and T. Liu, "Thermo-hydro-mechanical couplings controlling gas migration in heterogeneous and elastically-deformed coal," *Computers and Geotechnics*, vol. 123, p. 103570, 2020.

[16] W. Zhu, L. Liu, J. Liu, C. Wei, and Y. Peng, "Impact of gas adsorption-induced coal damage on the evolution of coal permeability," *International Journal of Rock Mechanics and Mining Sciences*, vol. 101, pp. 89–97, 2018.

[17] D. Wang, H. Ge, X. Wang, J. Wang, and F. Meng, *The Mechanical Properties of Gas Shale under Uniaxial Stress*, OnePetro, United States, 2015.

[18] D. Wang, H. Ge, B. Yu et al., "Study on the influence of elastic modulus heterogeneity on in-situ stress and its damage to gas shale reservoirs," *Journal of Natural Gas Geoscience*, vol. 3, no. 3, pp. 157–169, 2018.

[19] W. C. Zhu, J. Liu, T. H. Yang, J. C. Sheng, and D. Elsworth, "Effects of local rock heterogeneities on the hydromechanics of fractured rocks using a digital-image-based technique," *International Journal of Rock Mechanics and Mining Sciences*, vol. 43, no. 8, pp. 1182–1199, 2006.

[20] G. J. Chen, A. Ledesma, and L. Yu, "Simulation of thermo-hydro-mechanical (THM) coupled behaviour of a full scale in-situ test prototype repository," in *Soil and Rock Behavior and Modeling*, pp. 105–111, American Society of Civil Engineers, Shanghai, China, 2006.

[21] F. Dupray, C. Li, and L. Laloui, "THM coupling sensitivity analysis in geological nuclear waste storage," *Engineering Geology*, vol. 163, pp. 113–121, 2013.

[22] C.-S. Oh, N.-H. Kim, Y.-J. Kim, J.-H. Baek, Y.-P. Kim, and W.-S. Kim, "A finite element ductile failure simulation method using stress-modified fracture strain model," *Engineering Fracture Mechanics*, vol. 78, no. 1, pp. 124–137, 2011.

[23] Y. Wang, Z. Liu, H. Yang, Z. Shao, and Z. Zhuang, "FE analysis of rock with hydraulic-mechanical coupling based on continuum damage evolution," *Mathematical Problems in Engineering*, vol. 2016, 9 pages, 2016.

[24] E. Fjær, R. M. Holt, P. Horsrud, and A. M. Raaen, *Petroleum Related Rock Mechanics*, Elsevier, Amsterdam, Netherlands, 2008.